Inorganic Chemistry

Article

pubs.acs.org/IC

Slow Magnetic Relaxations in Cobalt(II) Tetranitrate Complexes. Studies of Magnetic Anisotropy by Inelastic Neutron Scattering and High-Frequency and High-Field EPR Spectroscopy

Lei Chen,[†] Hui-Hui Cui,[†] Shelby E. Stavretis,[‡] Seth C. Hunter,[‡] Yi-Quan Zhang,*[,§] Xue-Tai Chen,*[,†] Yi-Chen Sun,[∥] Zhenxing Wang,*[,∥] You Song,[†] Andrey A. Podlesnyak,*[,⊥] Zhong-Wen Ouyang,[∥] and Zi-Ling Xue*[,‡]

[†]State Key Laboratory of Coordination Chemistry, School of Chemistry and Chemical Engineering, Collaborative Innovation Center of Advanced Microstructures, Nanjing University, Nanjing 210023, People's Republic of China

[‡]Department of Chemistry, University of Tennessee, Knoxville, Tennessee 37996, United States

[§]Jiangsu Key Laboratory for NSLSCS, School of Physical Science and Technology, Nanjing Normal University, Nanjing 210023, People's Republic of China

[∥]Wuhan National High Magnetic Field Center, Huazhong University of Science and Technology, Wuhan 430074, People's Republic of China

[⊥]Quantum Condensed Matter Division, Oak Ridge National Laboratory, Oak Ridge, Tennessee 37831, United States

Supporting Information

ABSTRACT: Three mononuclear cobalt(II) tetranitrate complexes $(A)_2[Co(NO_3)_4]$ with different countercations, Ph_4P^+ (**1**), $MePh_3P^+$ (**2**), and Ph_4As^+ (**3**), have been synthesized and studied by X-ray single-crystal diffraction, magnetic measurements, inelastic neutron scattering (INS), high-frequency and high-field EPR (HF-EPR) spectroscopy, and theoretical calculations. The X-ray diffraction studies reveal that the structure of the tetranitrate cobalt anion varies with the countercation. **1** and **2** exhibit highly irregular seven-coordinate geometries, while the central Co(II) ion of **3** is in a distorted-dodecahedral configuration. The sole magnetic transition observed in the INS spectroscopy of **1**−**3** corresponds to the zero-field splitting $(2(D^2 + 3E^2)^{1/2})$ from 22.5(2) cm^{-1} in **1** to 26.6(3) cm^{-1} in **2** and 11.1(5) cm^{-1} in **3**. The positive sign of the D value, and hence the easy-plane magnetic anisotropy, was demonstrated for **1** by INS studies under magnetic fields and HF-EPR spectroscopy. The combined analyses of INS and HF-EPR data yield the D values as +10.90(3), +12.74(3), and +4.50(3) cm^{-1} for **1**−**3**, respectively. Frequency- and temperature-dependent alternating-current magnetic susceptibility measurements reveal the slow magnetization relaxation in **1** and **2** at an applied dc field of 600 Oe, which is a characteristic of field-induced single-molecule magnets (SMMs). The electronic structures and the origin of magnetic anisotropy of **1**−**3** were revealed by calculations at the CASPT2/NEVPT2 level.

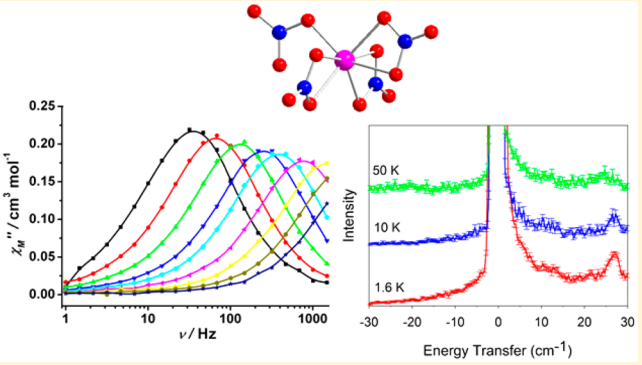

INTRODUCTION

Single-molecule magnets (SMMs), which are magnetic molecules showing slow magnetic relaxation and magnetic hysteresis below the critical temperature, have increasingly attracted attention due to their interesting magnetic properties and potential applications in ultrahigh-density storage and quantum computing in spintronics.[1−3] The SMM properties are associated with an energy barrier of U_{eff} for the reverse of the magnetic moment, which is governed by the total spin S and the easy-axis anisotropy parameter D via the relationship of $U_{eff} = |D|S^2$ for integer spins and $U_{eff} = |D|(S^2 - 1/4)$ for half-integer spins.[1−3] Increasing the total spin S of the ground state has been the main approach to achieve SMMs with superior properties in the past two decades. However, it has been found to be very difficult to simultaneously enhance both $|D|$ and S, because the easy-axis anisotropy parameter value $|D|$ is theoretically demonstrated to be inversely proportional to the square of the ground-state spin value (S^2).[4] There are many molecular systems with large ground spin without SMM properties. For instance, a ferromagnetically coupled Mn_{19} cluster with the spin ground state $S = 83/2$[5a] and an Fe_{42} cyanide-bridged nanocage with $S = 45$[5b] have very low magnetic anisotropy, which do not have the required energy barrier for

Received: June 28, 2016
Published: December 7, 2016

DOI: 10.1021/acs.inorgchem.6b01544
Inorg. Chem. 2016, 55, 12603−12617

an SMM. These experimental results and theoretical considerations have promoted the studies of SMMs with one highly anisotropic paramagnetic center including an f-[1d,6] and d-block ion.[7−18] They are commonly referred to as mononuclear single-molecule magnets or single-ion magnets (SIMs). Since the discovery of the first d-ion SIM based on low-coordinate high-spin iron(II) complexes by Long et al.,[10a,b] there have been a growing number of SIMs based on mononuclear d-ion complexes.[7−18] It is now a consensus that the coordination environment significantly affects the magnetic anisotropy in the d-ion SIMs: hence, the SIM properties.[7] It is believed that the low-coordination ligand field splits the d orbitals with a small separation between the electronic ground state and the excited states, facilitating the spin−orbital coupling and hence enhancing the magnetic anisotropy.[7] A very large effective energy barrier of U_{eff} = 226(4) cm^{-1}, which even surpasses that of the archetype Mn_{12} acetate SMM, has been reported for the two-coordinate Fe(I) complex $[K(crypt\text{-}222)][Fe(C(SiMe_3)_3)_2]$.[10c] In addition to the known d-ion SIMs containing Cr(II),[8] Mn(III),[9] Fe(I,II,III),[10] Ni(I,II),[11] and Re(IV)[12] ions, Co(II) SIMs constitute the largest family,[13−18] most of which have coordination numbers ranging from 2 to 6.[13−16] Recently, we reported the first eight-coordinate Co(II) SIM with a large axial zero-field splitting,[18] in which the central Co(II) ion is in a distorted-square-antiprismatic geometry. Subsequently several seven-coordinate Co(II) SIMs in the distorted-pentagonal-bipyramidal geometry have been reported to exhibit large positive anisotropy.[17] In addition, two seven-coordinate Fe(II) SIMs in the distorted-pentagonal-bipyramidal geometry with moderate, negative anisotropy were also reported.[10h,i] These SIMs clearly show that the high coordination geometry can also lead to the large magnetic anisotropy of Co(II) or Fe(II) if the donor atoms provide a weak ligand field. Due to the limited number of the known high-coordinate SIMs based on d-block ions, it is highly desirable to have more examples of high-coordinate SIMs in order to get an insight into the relationships among the coordination environment, local symmetry, magnetic anisotropy, and dynamic magnetic properties of SIMs.

In 1964, Bergman and Cotton reported the structural characterization of the first eight-coordinate Co(II) complex, $(AsPh_4)_2[Co(NO_3)_4]$.[19a,b] Afterward, Co(II) tetranitrate species with different countercations, $(A)_2[Co(NO_3)_4]$ (cation A^+ = Na^+, K^+, Cs^+, NO^+), were shown to have different coordination geometries.[20] It is reasoned that the coordination environment affects the ligand field, resulting in the different magnetic anisotropies and dynamic magnetic properties. The nitrate group is a ligand exhibiting very weak ligand field strength,[19c] which would probably give rise to high-spin homoleptic Co(II) nitrate complexes with large magnetic anisotropy. The variation of coordination geometry for $[Co(NO_3)_4]^{2-}$ anions with countercations has inspired us to study the magnetic properties of Co(II) tetranitrate complexes. As part of our research into d-ion SIMs with high coordination numbers, here we report the structural and magnetic studies of three cobalt(II) complexes with $[Co(NO_3)_4]^{2-}$ anions: $(PPh_4)_2[Co(NO_3)_4]\cdot CH_2Cl_2$ (**1**), $(MePPh_3)_2[Co(NO_3)_4]$ (**2**), and $(AsPh_4)_2[Co(NO_3)_4]$ (**3**). Inelastic neutron scattering (INS), high-frequency and high-field EPR (HF-EPR) spectroscopy, and theoretical calculations have been used to probe the nature and magnitude of the magnetic anisotropies in **1**−**3**.

EXPERIMENTAL SECTION

The reagents employed were commercially available and used without further purification. All manipulations were performed using standard Schlenk techniques under an N_2 atmosphere. Acetonitrile (MeCN), dichloromethane (CH_2Cl_2), and hexanes were dried and purified using conventional methods before use. Elemental analyses were performed on an Elementar Vario ELIII elemental analyzer. The infrared spectra were measured on a Tensor 27 FT-IR spectrometer using KBr pellets in the range of 400−4000 nm. Powder X-ray diffraction (PXRD) patterns were recorded on a Bruker D8 ADVANCE X-ray powder diffractometer in the 2θ range of 5−50° at room temperature. PXRD patterns show that the samples of **1**−**3** for magnetic measurements and INS and HF-PER studies are monophase crystalline materials (Figures S1−S3 in the Supporting Information). **1**−**3** were prepared by a method similar to that of Bergman and Cotton.[19a]

Synthesis of $(PPh_4)_2[Co(NO_3)_4]\cdot CH_2Cl_2$ (1). A solution of $AgNO_3$ (2.0 mmol, 0.340 g) in 10 mL of CH_3CN was added to a solution of tetraphenylphosphonium chloride (1.0 mmol, 0.375 g) and $CoCl_2$ (0.5 mmol, 0.065 g) in 10 mL of CH_3CN. The resulting solid AgCl was separated, and the filtrate was concentrated to give a microcrystalline solid by evaporation. The pink block crystals of **1** were obtained in 81% yield by recrystallization of the crude product in dichloromethane−hexane at −10 °C for several days. IR (KBr, cm^{-1}): 3406 (br), 1641 (br), 1585 (w), 1466 (m), 1435 (ms), 1396 (s), 1384 (m), 1311 (s), 1292 (m), 1188 (w), 1163 (w), 1108 (s), 1027 (w), 1016 (w), 996 (w), 812 (w), 757 (m), 722 (s), 690 (s), 536 (sh), 527 (s). Anal. Calcd for $C_{48}H_{40}CoN_4O_{12}P_2$ (analysis for the dry sample without solvent CH_2Cl_2): C, 58.49; H, 4.09; N, 5.68. Found: C, 58.11; H, 4.20; N, 5.60.

Synthesis of $(MePh_3P)_2[Co(NO_3)_4]$ (2). **2** was prepared by the same procedure as **1**, but using methyltriphenylphosphonium bromide (1.0 mmol, 0.357 g) instead of tetraphenylphosphonium chloride (1.0 mmol, 0.375 g). The pink block crystals of **2** were obtained in 80% yield. IR (KBr, cm^{-1}): 3428 (s), 3061 (w), 2982 (w), 2908 (w), 2853 (w), 1638 (m), 1590 (w), 1485 (sh), 1463 (s), 1440 (s), 1396 (m), 1364 (s), 1319 (m), 1291 (m), 1115 (m), 1024 (w), 996 (w), 910 (w), 900 (m), 747 (s), 720 (m), 689 (s), 500 (m). Anal. Calcd for $C_{38}H_{36}CoN_4O_{12}P_2$: C, 52.97; H, 4.21; N, 6.50. Found: C, 52.64; H, 4.29; N, 6.48.

Synthesis of $(AsPh_4)_2[Co(NO_3)_4]$ (3). **3** was prepared by the same procedure as **1**, but with tetraphenylarsonium chloride (1.0 mmol, 0.420 g) instead of tetraphenylphosphonium chloride (1.0 mmol, 0.375 g). The pink block crystals of **3** were obtained in 73% yield. IR (KBr, cm^{-1}): 3413 (b), 2362 (w), 1654 (w), 1636 (w), 1466 (s), 1437 (s), 1395 (m), 1323 (m), 1286 (m), 1187 (w), 1079 (m), 1018 (m), 995 (m), 813 (w), 747 (s), 737 (s), 479 (m), 470 (m), 454 (w). Anal. Calcd for $C_{48}H_{40}CoN_4O_{12}As_2$: C, 53.70; H, 3.76; N, 5.22. Found: C, 53.38; H, 3.82; N, 5.17.

X-ray Single-Crystal Structure Determination. X-ray diffraction intensities were collected for **1**−**3** using a Bruker APEX DUO diffractometer at 296 K with a CCD area detector (Mo Kα radiation, λ = 0.71073 Å).[21] The APEXII program was used for collecting frames of data and determining lattice parameters. SAINT was used to integrate the data. The absorption corrections were applied using SADABS.[22] The structures were solved using SHELXS-97 and subsequently completed via Fourier recycling using the SHELXL-97 program.[23] The Co atom of each compound was determined first, and O, N, and C atoms were subsequently identified using the difference Fourier maps. All non-hydrogen atoms were refined with anisotropic thermal parameters, and hydrogen atoms were set at calculated positions and generated by the riding model.

Magnetic Measurements. Direct-current (dc) magnetic data of **1**−**3** were recorded at fields up to 7 T with a Quantum Design MPMS-XL17 SQUID instrument in the range of 1.8−300 K. Alternating-current (ac) susceptibility measurements were carried out using an oscillating ac field of 5 Oe and ac frequencies ranging from 1 to 1500 Hz under different applied static fields. The measurements were performed with the polycrystalline samples of **1**−**3** restrained in Parafilm. The magnetic susceptibility data were corrected for the

DOI: 10.1021/acs.inorgchem.6b01544
Inorg. Chem. 2016, 55, 12603−12617

sample holder as well as for diamagnetism of the constituent atoms (estimated using Pascal's constants).

Inelastic Neutron Scattering (INS) Studies. The INS measurements were carried out on the Cold Neutron Chopper Spectrometer (CNCS),[24] Spallation Neutron Source at Oak Ridge National Laboratory. CNCS is a direct geometry, time-of-flight spectrometer that receives a beam from a coupled cryogenic H_2 moderator. For energy selection, CNCS employs four chopper assemblies. The speeds and slit widths of the choppers may vary, allowing adjustments in the instrumental resolution and intensity of the incident beam. Approximately 500 mg of each sample was loaded into a 1/2 in. thick aluminum tube. For the INS work without a magnet, three tubes containing $(A)_2[Co(NO_3)_4]$ were placed in a sample changer. The sample holder was mounted in a standard liquid helium cryostat with a base temperature of T = 1.6 K. An oscillating radial collimator was used to reduce background scattering form the tail of the cryostat. Vanadium was used as a standard for the detector efficiency correction.

The incident neutron energy for every measurement was chosen to cover the anticipated region of interest in both the energy E and scattering-vector $\mathbf{Q}$ space. A small incident energy is especially important to observe excitations near the elastic peak (at energy transfer close to 0 cm^{-1}) as the full width at half-maximum (fwhm) of the elastic peak, which is typically 1.5−2% of the incident energy, would be narrow, giving better energy resolution.

For **1**, zero-field measurements were performed at 1.7, 5, 10, 20, 30, 50, and 100 K with an incident neutron energy of 53.7 cm^{-1}. For **2** and **3**, measurements were performed at 1.6, 10, and 50 K with incident neutron beam energies of 24.2 and 40.3 cm^{-1}. Data were then reduced and analyzed using the MantidPlot[25a] and DAVE (data analysis and visualization environment) program package.[25b]

Another INS experiment for the powder sample of **1** was performed at 1.7 K using a 5 T cryomagnet with vertical field at CNCS. An aluminum spacer was added to the headspace of the sample can to prevent the sample reorientation in the applied field. Magnetic fields at 0.5, 1.0, and 2.0 T were used with an incident neutron energy of 13.4 cm^{-1}. The cryomagnet sample room allows only one sample at a given time.

The neutron magnetic scattering cross-section[26] corresponds to the number of neutrons scattered per second, due to the magnetic interaction, into a solid angle $d\Omega$ with energy transfer between $\hbar\omega$ and $\hbar(\omega + d\omega)$, divided by the flux of the incident neutrons. For unpolarized neutrons, identical magnetic ions with localized electrons, and spin-only scattering, the magnetic scattering cross-section is expressed by eq 1:[26]

$$\frac{d^2\sigma}{d\Omega\, d\omega} = (\gamma r_0)^2 \frac{k_f}{k_i}\left[\frac{1}{2}gF(Q)\right]^2 e^{-2W(Q)} \sum_{\alpha,\beta}\left(\delta_{\alpha,\beta} - \frac{Q_\alpha - Q_\beta}{Q^2}\right) \times S^{\alpha,\beta}(Q,\omega) \quad (1)$$

where σ = neutron cross section, γ = gyromagnetic ratio, r_0 = classical radius of an electron, g = Landé g factor, $F(\mathbf{Q})$ = dimensionless magnetic form factor defined as the Fourier transform of the normalized spin density associated with magnetic ions, $e^{-2W(\mathbf{Q})}$ = Debye−Waller factor caused by thermal motion, $S^{\alpha\beta}(Q,\omega)$ = magnetic scattering function, $\delta_{\alpha,\beta} - (Q_\alpha Q_\beta)/Q^2$ = polarization factor which implies neutrons can only couple to magnetic moments or spin fluctuations perpendicular to $\mathbf{Q}$, $\hbar\omega$ = energy change experienced by the sample, and ω = angular frequency of neutron.

The line widths of the INS peaks lie within experimental accuracy determined by the instrumental resolution. The effective resolution function $R(Q,E)$ of CNCS is nearly Gaussian in energy.[24] Therefore, the INS intensities were fit assuming Gaussian line shapes with fwhm of the energy resolution for the CNCS spectrometer. Additional details of data processing are provided in the Supporting Information.

HF-EPR Measurements. HF-EPR measurements for **1**−**3** were performed on a locally developed spectrometer at the Wuhan National High Magnetic Field Center, People's Republic of China.[27,28] This facility is a transmission-type instrument, in which the microwaves are propagated by oversized cylindrical lightpipes. The tunable microwave frequencies were provided by the combination of Gunn oscillators (Millitech) and backward wave oscillators (Institute of General Physics, Moscow, Russian Federation). The magnetic field was generated by a pulsed field magnet, and the detection was performed with an InSb hot-electron bolometer (QMC Ltd., Cardiff, U.K.). In order to minimize the field-induced torquing effect, samples of **1**−**3** were ground, mixed with KBr, and pressed into pellets.

Computational Details. *CASPT2.* Complete active space second-order perturbation theory (CASPT2), considering the effect of the dynamic electronic correlation based on complete active space self-consistent field (CASSCF) using the MOLCAS 8.0 program package,[29] was performed on the complete structures of **1**−**3**. For the first CASSCF calculation, the basis sets for all atoms were atomic natural orbitals from the MOLCAS ANO-RCC library: ANO-RCC-VTZP for magnetic center ion Co^{II}, VTZ for close O, and VDZ for distant atoms. The calculations employed the second-order Douglas−Kroll−Hess Hamiltonian, where scalar relativistic contractions were taken into account in the basis set. After that, the effect of the dynamic electronic correlation was applied using CASPT2. Then the spin−orbit coupling was handled separately in the restricted active space state interaction (RASSI-SO) procedure. The active electrons in 10 active spaces considering the 3d double shell effect (5 + 5′) include all seven 3d electrons, and the number of mixed spin-free states is 50 (all from 10 quadruplets; all from 40 doublets).

NEVPT2. To deeply analyze the magnetic anisotropy of complexes **1**−**3**, ORCA 3.03 calculations[30] were performed with the n-electron valence state perturbation theory (NEVPT2)[31] method. The spin−orbit coupling (SOC) operator used was the efficient implementation of the multicenter spin−orbit mean-field (SOMF) concept developed by Hess et al.[32] The spin−spin contributions (SSC) to the D values were also included, although they are very small for our complexes. The first CASSCF calculation with 7 3d electrons in the 10 Co 3d-based orbitals (CAS(7, 10)) were performed on complexes **1**−**3**, and then NEVPT2[31] on top of the CAS(7, 10) reference states was carried out. In the calculations, the orbitals were determined for the average of 10 S = 3/2 and 40 S = 1/2 roots. All calculations were performed with a triple-ζ with one polarization function (TZVP[33]) basis set for all atoms. Tight convergence criteria were used in order to ensure that the results are well converged with respect to technical parameters. The effective Hamiltonian implemented in ORCA was used to extract the ZFS parameters D and E.

RESULTS AND DISCUSSION

Structural Features of 1−3. The structural data of **3** with a low precision (R = 0.12) were reported earlier in 1964 by Bergman et al.[19a] Here its structure was redetermined with higher quality along with the structures of **1** and **2** by X-ray crystallography. Table S1 in the Supporting Information gives the parameters of single-crystal structural analyses for **1**−**3**. **1** and **2** crystallize in the triclinic space group $P\bar{1}$, while **3** crystallizes in monoclinic space group $C2/c$. The structures of the anions of **1**−**3** are depicted in Figure 1. Selected bond lengths and angles of **1**−**3** are given in Table 1.

The anions of **1** and **2** exhibit a highly irregular seven-coordinate geometry, in which the central Co(II) ion is coordinated by seven oxygen atoms originating from one monodentate and three unsymmetrical bidentate NO_3^- groups,[34] as reported for $Cs_2[Co(NO_3)_4]$.[20b] The Co−O distances of three bidentate NO_3^- ligands in **1** are varied, which can be classified as two sets: three shorter Co−O distances (Co(1)−O(5), 2.041(3); Co(1)−O(7), 2.126(4) Å; Co(1)−O(11), 2.066(4)) and three longer distances (Co(1)−O(4), 2.517(5); Co(1)−O(8), 2.308(4); Co(1)−O(10), 2.396(4) Å). The monodentate NO_3^- group coordinates to Co(II) with the shortest Co−O distance (Co(1)−O(11), 2.034(4) Å) and a long nonbonding Co(1)···O(3) distance (2.820(5) Å). In **2**, the Co−O bond distances from the three unsymmetrical bidentate

DOI: 10.1021/acs.inorgchem.6b01544
Inorg. Chem. 2016, 55, 12603−12617

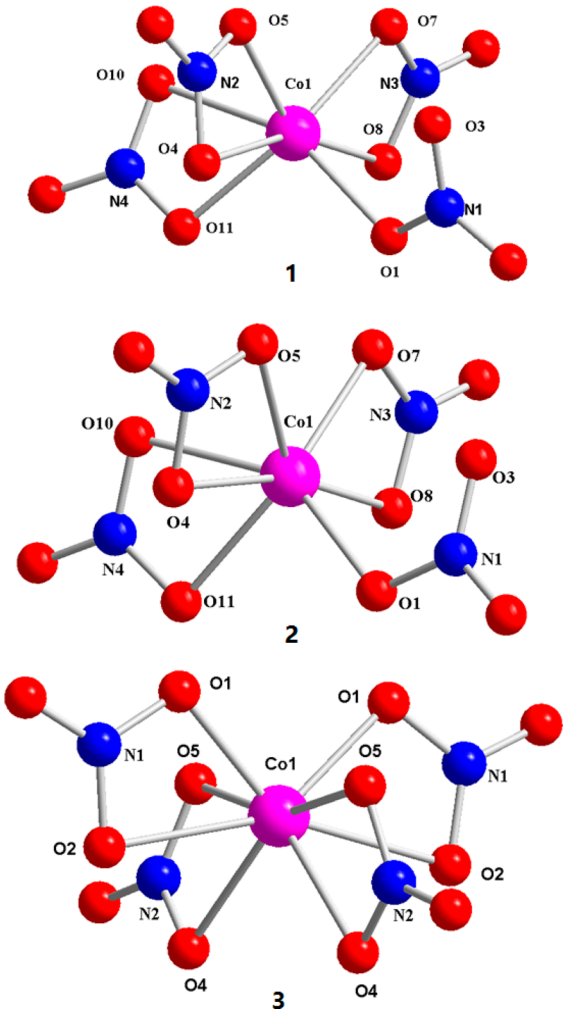

Figure 1. Structures of the anions $[Co(NO_3)_4]^{2-}$ in **1**–**3**. Pink, red, and blue spheres represent Co, O, and N atoms, respectively. H atoms are omitted for clarity. Only one set of the two disordered nitrate groups centered around the N(2) atom is shown in **3** for clarity.

NO_3^- groups can also be divided into three shorter Co–O and three longer Co–O distances, but they are not as differentiated as in **1** (Table 1). The Co–O distances vary from 2.146(2) to 2.307(3) Å with an average bond distance of 2.205(2) Å. As in **1**, the monodentate NO_3^- gives the shortest Co–O bond (2.035(2) Å) and a nonbonding Co(1)···O(3) distance of 2.772(8) Å. The ranges of the interior O–Co–O angles in bidentate NO_3^- groups in **1** and **2** are 53.53(16)–56.26(17) and 54.35(11)–57.13(9)°, respectively.

As determined previously in 1964,[19] the Co(II) ion in **3** is coordinated by eight oxygen atoms from four unsymmetrical bidentate NO_3^- groups (O4–N–O5)[34] to form a distorted-dodecahedral configuration (Figure 1). Two symmetrically related NO_3^- groups centered around N(2) atom are disordered at two positions. The local structural symmetry of **3** is C_2 but is close to D_{2d} symmetry. We have performed continuous shape measure (CSM) analyses[35] with regard to several ideal polyhedrons such as pentagonal bipyramid, capped trigonal prism, capped octahedron, heptagon, and hexagonal pyramid for **1**–**3** (Table S2 in the Supporting Information). No suitable approximate seven-vertex geometries were obtained in **1** and **2**, further indicating their irregular structures. However, the CSM analyses show that the structure of **3** is close to a triangular dodecahedron. Obviously **3** is more regular and symmetric than **1** and **2**. The shortest intermolecular Co···Co distances are 9.4685(20), 10.7563(12), and 9.9898(14) Å, respectively, in **1**–**3**. Furthermore, there is no significant contact among the ligands of the neighboring molecules.

Static Magnetic Properties. Variable-temperature direct-current (dc) magnetic susceptibilities were measured for polycrystalline samples of **1**–**3** at a field of 2000 Oe in the temperature range of 1.8–300 K. The resulting $\chi_M T$ versus T curves are shown in Figure 2. At room temperature, the $\chi_M T$

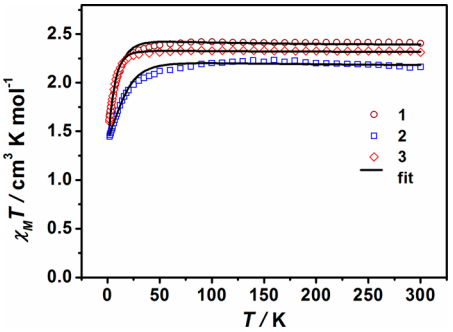

Figure 2. Variable-temperature dc susceptibility data under an applied dc field of 2000 Oe for **1**–**3**. Solid black lines indicate the best fits with the PHI program.[36]

Table 1. Selected Bond Lengths (Å) and Angles (deg) for 1–3

1		2		3	
Co–O(1)	2.034(4)	Co–O(1)	2.035(2)	Co–O(1)	2.071(2)
Co–O(4)	2.517(5)	Co–O(4)	2.260(2)	Co–O(2)	2.437(2)
Co–O(5)	2.041(3)	Co–O(5)	2.235(2)	Co–O(4)	2.046(9)
Co–O(7)	2.125(4)	Co–O(7)	2.146(2)	Co–O(5)	2.15(2)
Co–O(8)	2.308(5)	Co–O(8)	2.218(2)		
Co–O(10)	2.396(4)	Co–O(10)	2.307(3)		
Co–O(11)	2.066(4)	Co–O(11)	2.236(2)		
Co···O(3) (nonbonding)	2.820(5)	Co···O(3) (nonbonding)	2.772(8)		
O4–Co–O5	53.66(14)	O4–Co–O5	54.35(11)	O1–Co–O2	54.83(9)
O7–Co–O8	56.23(19)	O7–Co–O8	57.13(9)		
O10–Co–O11	55.38(15)	O10–Co–O11	55.70(10)		

DOI: 10.1021/acs.inorgchem.6b01544
Inorg. Chem. 2016, 55, 12603–12617

values are 2.41, 2.16, and 2.31 cm^3 K mol^{-1}, consistent with an $S = 3/2$ spin center with $g = 2.27$, 2.15, and 2.22 for **1**−**3**, respectively. These values show a significant decrease below 60, 130, and 50 K for **1**−**3**, reaching values of 1.65, 1.45, and 1.60 cm^3 K mol^{-1} at 1.8 K, respectively. In the absence of intermolecular magnetic interactions as judged by the long Co···Co distances and no significant contacts among the ligands, this decline at low temperature is attributed to the intrinsic magnetic anisotropies of the Co(II) ions in **1**−**3**.

The field-dependent magnetizations were measured for **1**−**3** at applied magnetic fields in the range of 1−7 T at 1.8 K (Figure S4 in the Supporting Information). The magnetizations do not reach saturation at 7 T with 2.44, 2.30, and 2.58 N_β for **1**−**3**, respectively. Low-temperature magnetization data from 1.8 to 5.0 K at various applied dc fields were also measured for **1**−**3** (Figures S5−S7 in the Supporting Information). Non-saturation of magnetization at 7 T and the nonsuperposition of M versus H/T curves suggest the presence of significant magnetic anisotropies in **1**−**3**. To estimate the zero-field splitting parameters D and E, the $\chi_M T$ versus T and M versus H/T curves at different temperatures were simultaneously fitted using the PHI program[36] by the anisotropic spin Hamiltonian (SH) (with $g_x = g_y$) as given in eq 2, which includes the axial/rhombic ZFS and Zeeman interactions:

$$H = D(\hat{S}_z^{\,2} - S(S+1)/3) + E(\hat{S}_x^{\,2} - \hat{S}_y^{\,2}) + \mu_B g\hat{S}\cdot\hat{H} \quad (2)$$

where μ_B is the Bohr magneton and D, E, S, and H represent the axial and rhombic ZFS parameters, the spin operator, and magnetic field vectors, respectively.

The best fits afforded the parameters for **1**−**3** in Table 2. The signs of axial ZFS parameters D for **1**−**3** are positive. The D value for **3** is smaller than those for **1** and **2**, probably due to the different coordination environments of **1** and **2** in comparison to **3**. It is known that dc magnetic data usually cannot yield accurate values for D and E, especially their signs. Therefore, HF-EPR and INS studies have been performed to further investigate their magnetic anisotropy.

Table 2. Zero Splitting Parameters Obtained Experimentally for Complexes 1−3

	1	2	3
Fitting of the dc Magnetic Data by PHI[36]			
D, cm^{-1}	12.85	23.21	7.95
E, cm^{-1}	3.60	0.64	1.88
g_z	2.41	2.29	2.03
$g_{x,y}$	1.89	1.83	2.31
Data from INS Measurements			
$2(D^2 + 3E^2)^{1/2}$, cm^{-1}	22.5(2)	26.6(3)	11.1(5)
Data from INS/HF-EPR Measurements			
D, cm^{-1}	10.90(2)	12.74(2)	4.50(3)
E, cm^{-1}	1.56(2)	2.20(2)	1.00(2)
g_z	2.39(1)	2.20(1)	2.40(2)
$g_{x,y}$	2.23(1)	2.21(1)	2.30(2)

INS Studies. Inelastic neutron scattering (INS) has been used to probe the magnetic properties of metal complexes, especially excitations among low-lying energy levels.[37] Most of the INS studies were limited to paramagnetic metal clusters,[26,37,38] and a few reports have been published on mononuclear metal complexes,[39] including one Co(II)-based[16a] and one Re(IV)-based[12b] SIM.

To further investigate the magnetic anisotropy, the polycrystalline samples of **1**−**3** were studied by INS. Data for **1** were collected at varying temperatures to observe the sole ZFS transition for the $S = 3/2$ system. The resulting energy spectrum exhibits a peak associated with transitions from $M_s = \pm 1/2$ to $\pm 3/2$ (Scheme 1). The splitting between the two Kramers doublets is $2(D^2 + 3E^2)^{1/2}$. (It is $2D$ for the axial symmetrical system when $E = 0$.) In the INS spectra of **1**, a peak at 22.5(2) cm^{-1} is observed with an incident energy of 53.7 cm^{-1} (Figure 3 and Figure S8 and Table S3 in the Supporting Information). As the temperature is increased from 1.7 to 100 K, the population in the ground state is decreased, leading to a less intense transition. At 50 K, a peak at −22.5(2) cm^{-1} is observed, indicating that the incident neurons gain energy from the sample in the INS process. During the scattering process, those molecules return to the ground state, transferring the energy to the neutrons. Therefore, the zero-field splitting value of $2(D^2 + 3E^2)^{1/2}$ was determined to be 22.5(2) cm^{-1} for **1** from the sole magnetic transition. Peaks of magnetic excitations fall off with increasing |Q|, as a result of the decrease in the distribution of spin and orbital magnetization from unpaired electrons. The opposite is true for peaks of the vibrational origin which increase in intensity with |Q|. The decrease in magnetic excitations follows the square of the magnetic form factor $F(\mathbf{Q})$ in eq 1. Additional information about the magnetic peak in the INS spectra of **1** is provided by 2-D scattering intensities vs |Q| plots in Figure S13 in the Supporting Information.

In order to determine the sign of the D parameter in **1**, further INS measurements were performed under a magnetic field, which leads to additional splitting ($\Delta M_S = \pm 1$) of the original ZFS transition, as shown in Scheme 1. If $D > 0$, an additional magnetic transition, $M_S = -1/2 \rightarrow +1/2$, would be observed at low energy and low temperatures (Scheme 1, left). However, if $D < 0$, the first magnetic transition, $M_S = -3/2 \rightarrow +3/2$, would be forbidden (Scheme 1, right).

Scheme 1. (Left) ZFS Energy Diagram, $D > 0$, with the Application of a Magnetic Field and (Right) ZFS Energy Diagram, $D < 0$, with the Application of a Magnetic Field

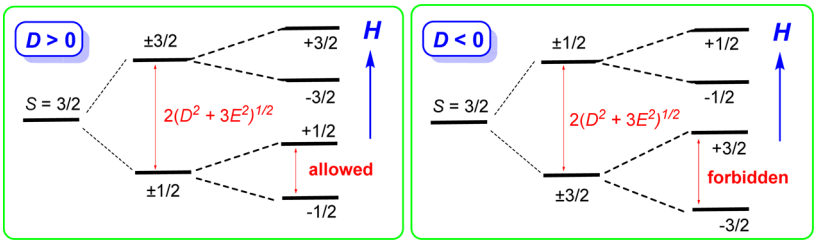

DOI: 10.1021/acs.inorgchem.6b01544
Inorg. Chem. 2016, 55, 12603−12617

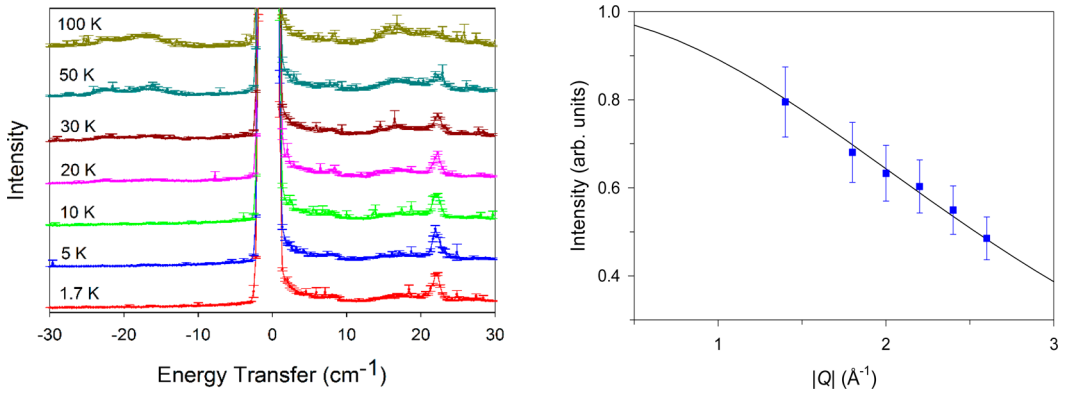

Figure 3. (left) INS spectra of **1** with incident neutron energy E_i = 53.7 cm^{-1}, |Q| = 0.5−1.3 Å^{-1}, and a step size of 0.081 cm^{-1}. (right) Change in intensities of the magnetic peak at 22.5(2) cm^{-1} vs |Q| at 1.7 K. The solid line represents the calculated intensity of the magnetic excitation.

Measurements for **1** were taken at 0.0, 0.5, 1.0, and 2.0 T at 1.7 K. The incident energy of 13.4 cm^{-1} was used to see if the magnetic transition, $M_S = -1/2 \rightarrow +1/2$, would be observed at low temperatures (Scheme 1, left). An excitation appeared at 2.0 cm^{-1} when a 2 T magnetic field was applied (Figure 4 and Figure S11 and Table S6 in the Supporting Information). This peak confirms easy-plane anisotropy in **1**. It should be noted that the 5 T magnet, added inside the sample environment in CNCS, blocks some neutron detectors and itself scatters neutrons to other detectors as background noise. Thus, the signal to noise ratio in Figure 4 is significantly reduced.

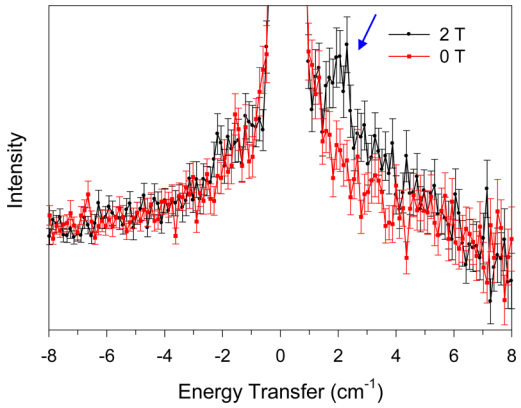

Figure 4. INS spectra of **1** at 1.7 K, showing the $M_S = -1/2 \rightarrow +1/2$ transition at 2 T (indicated by the blue arrow) with an incident neutron energy of E_i = 13.4 cm^{-1} and |Q| = 0.4−1.3 Å^{-1}. The solid lines are for guides for the eye.

INS studies are usually performed to probe the magnetic excitations in molecular magnetism with zero magnetic field. The application of a magnetic field is expected to lead to more information about the compound, as shown in this study. Only limited studies of INS under applied magnetic fields have been reported, which were focused on the magnetic clusters Cr_8, Fe_9, $Mo_{72}Fe_{30}$, and Cr_7Ni[40] and low-dimensional antiferromagnets.[41] To the best of our knowledge, such INS under magnetic fields has not been performed on mononuclear metal complexes including SIMs. Our study here provides the first example using INS with magnetic fields to determine the sign of magnetic anisotropy for a mononuclear metal complex.

In the INS spectrum of **2**, a peak at 26.6 cm^{-1} was observed with an incident energy of 40.3 cm^{-1} (Figure 5 and Figure S9 and Table S4 in the Supporting Information). From INS measurements the zero-field splitting $2(D^2 + 3E^2)^{1/2}$ was determined as 26.6(3) cm^{-1}. In the INS spectra of **3**, a peak at 11.1(5) cm^{-1} was observed with an incident energy of 24.2 cm^{-1} representing $2(D^2 + 3E^2)^{1/2}$ (Figure 6 and Figure S10 and Table S5 in the Supporting Information). The ZFS transitions of **2** and **3** are of magnetic nature due to their temperature dependence and decreasing |Q| dependence, as observed in Figures 5 and 6. An additional plot showing how the magnetic peak in the INS spectrum of **3** at 1.7 K changes in two different |Q| ranges is given in Figure S14 in the Supporting Information.

It is interesting to note that a broad optical phonon peak centered around 18 cm^{-1}, even at 1.7 K, is present and is very

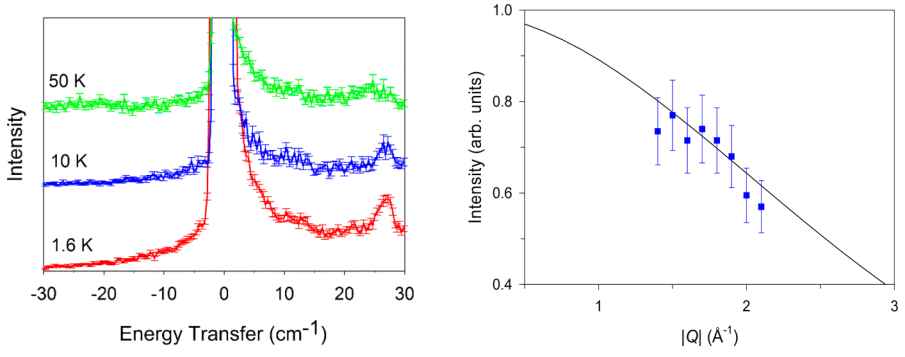

Figure 5. (left) INS spectra of **2** with incident neutron energy E_i = 40.33 cm^{-1}, |Q| = 0.5−1.3 Å^{-1}, and a step size of 0.081 cm^{-1}. (right) Change in intensities of the magnetic peak at 26.6 cm^{-1} vs |Q| at 1.6 K. The solid line represents the expected intensity of the peak calculated from the magnetic form factor.

DOI: 10.1021/acs.inorgchem.6b01544
Inorg. Chem. 2016, 55, 12603−12617

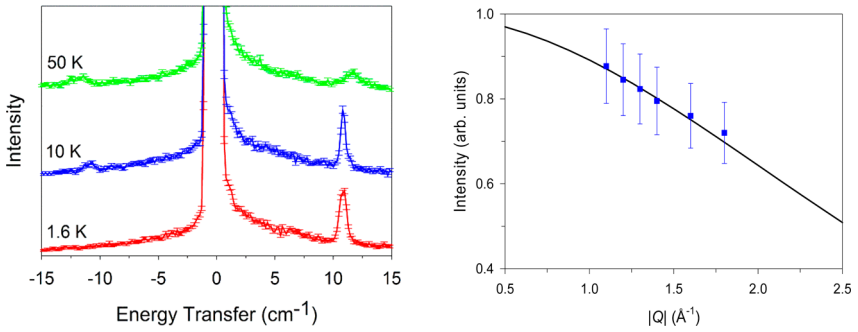

Figure 6. (left) INS spectra of **3** with the incident neutron energy of E_i = 24.2 cm^{-1}, |Q| = 0.5−2.0 $Å^{-1}$, and a step size of 0.081 cm^{-1}. (right) Change in intensities of the magnetic peak at 11.1(5) cm^{-1} vs |Q| at 1.6 K. The solid line represents the expected intensity of the peak calculated from the magnetic form factor.

close to the ZFS transition of **1** (Figure 3). The intensity of this peak increases quadratically with |Q|, as shown in Figure S12 in the Supporting Information, confirming its phonon nature. No such phonon peak near the magnetic peak is obvious in the INS spectra of **2** (Figure 5).

HF-EPR Studies. The above INS analysis shows that the values of zero-field splitting $2(D^2 + 3E^2)^{1/2}$ are 22.5, 26.6, and 11.1 cm^{-1} for **1**−**3**, respectively. However, the D and E values could not be separately determined from the sole INS transition. In order to determine the sign and values of D and E, the polycrystalline samples of **1**−**3** were investigated by high-frequency and high-field electron paramagnetic resonance (HF-EPR)[42] in the frequency range of 60−350 GHz, as shown in Figure 7. No EPR signals with reliable turning points were obtained beyond 250 GHz for **1** and **2** and beyond 350 GHz for **3**, probably due to the low sensitivity of our spectrometer in the high-frequency range. The HF-EPR spectra of **1** and **2** contain three main features, typical for a S = 3/2 system with large and positive D values,[14a,c,16a,c,17c,43,44a] which are from the intra-Kramers transitions within the M_S = ±1/2 doublets. The resonance fields at various microwave frequencies are extracted and plotted in Figure 8 as squares. The data branches are identified with theoretical simulations.[45] By using the constraint imposed by the values of $2(D^2 + 3E^2)^{1/2}$ obtained by INS, the field vs frequency data were fitted to give the spin Hamiltonian parameters in Table 2. In addition, the signs of D values were confirmed to be positive by comparing the simulated spectra with experimental EPR spectra in Figure 7.

The HF-EPR spectra were also recorded for **3** at 4.2 K. The curve of resonance fields at various microwave frequencies was established and plotted in Figure 8 as squares, which was simulated using the constrained value (11.1 cm^{-1}) of $2(D^2 + 3E^2)^{1/2}$. Again, if the sign of D was assigned as negative, no reasonably simulated spectra was obtained, confirming the positive sign of D in **3** (Figure 7).

The combination of INS and HF-EPR studies discussed above clearly demonstrates the easy-plane magnetic anisotropy in the high-coordinate Co(II) complexes **1**−**3**. A similar approach has been used to determine the D and E values for an Re(IV) SIM by Pedersen et al.[12b] The D values in Table 2 from INS and HF-EPR are smaller than those from the fitting of the dc magnetic data, suggesting that the D values were overestimated by the magnetic data.

Seven- and eight-coordinate 3d metal complexes are well known, but their magnetic properties have been rarely studied.[17,18,44,46] The seven-coordinate Co(II) complexes with a distorted-pentagonal-bipyramidal geometry exhibit positive

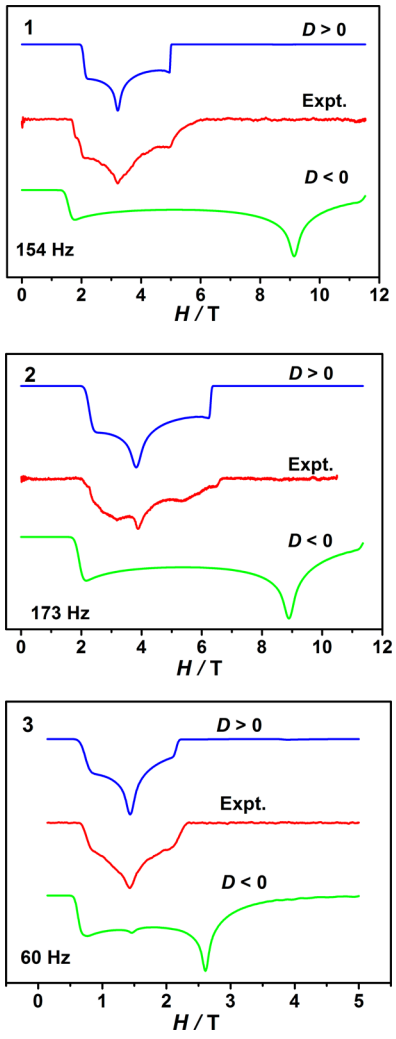

Figure 7. Representative HF-EPR spectra of **1**−**3** at 4.2 K (red) with their simulations (blue, D > 0; green, D < 0). The spin Hamiltonian parameters used for the simulations[45] are shown in Table 2.

magnetic anisotropy.[17,44] **1** and **2** here are seven-coordinated with highly irregular geometry and also have easy-plane magnetic anisotropy. The eight-coordinate compound **3** also exhibits positive anisotropy. It is noted that the only reported study of magnetic anisotropy of an eight-coordinate Co(II) complex was on $[Co(12\text{-crown-}4)_2](I_3)_2(12\text{-crown-}4)$ with negative anisotropy,[18] in which the Co^{II} ion is in a distorted-square-antiprismatic geometry. The coordination geometry of **3**

DOI: 10.1021/acs.inorgchem.6b01544
Inorg. Chem. 2016, 55, 12603−12617

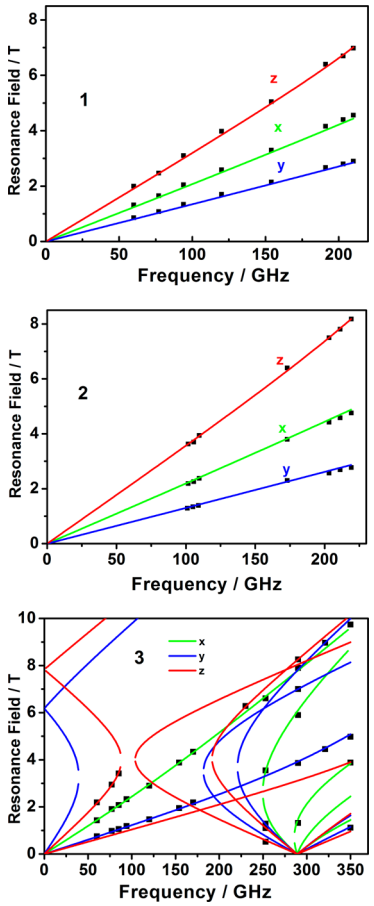

Figure 8. Resonance field vs microwave frequency for EPR transitions for **1**−**3**. Simulations[45] were conducted with the Hamiltonian parameters in Table 2. Solid lines show the (*x*, *y*, *z*) transitions as labeled.

is a distorted dodecahedron, another configuration for an eight-coordinate Co(II) complex. The different natures of the magnetic anisotropies of **3** and $[Co(12\text{-crown-}4)_2](I_3)_2(12\text{-crown-}4)$ are probably due to their different coordination environments.

Dynamic Magnetic Properties. It is generally accepted that a negative zero-field splitting is required for the single-molecule magnetism.[1,2] In 2012, Long et al.[14a] first observed the slow magnetic relaxation in a four-coordinate Co(II) complex with easy-plane anisotropy. Subsequently several SIMs with $S = 3/2$ ions, including Co(II)[14a−e,15g,16a−e,17] and Re(IV),[12b] have been reported to have positive D values. In order to investigate single-molecule magnetism for **1**−**3**, temperature- and frequency-dependent alternating-current (ac) susceptibility measurements were performed. At 1.8 K, no out-of-phase ac susceptibility (χ_M'') signal was observed for **1** and **2** under zero applied dc field (Figures S13 and S14 in the Supporting Information), which is probably due to the occurrence of quantum tunneling of the magnetization (QTM). The application of an external magnetic field could induce the strong frequency-dependent ac susceptibilities (Figures S13 and S14). For **1**, the maximum of χ_M'' appeared at 200 Oe, which shifted to low frequencies with an increase in the applied magnetic field up to 600 Oe and then stayed at the nearly same frequency as the magnetic field increased further. Therefore, a magnetic field of 600 Oe was used in temperature- and frequency-dependent ac measurements in the temperature range of 1.8−7.0 K (Figure 9 and Figures S15 and S16 in the Supporting Information). The temperature and frequency dependence of ac susceptibility signals indicates that both **1** and **2** exhibit slow magnetic relaxation processes and thus behave as field-induced SMMs. As shown in Figure 9, the peaks of χ_M'' signals for **1** and **2** appear at 398 and 35 Hz, respectively, at 1.8 K, suggesting that the magnetic relaxation is faster in **1** than in **2**.

In contrast with **1** and **2**, no significant out-of-phase signals (χ''_M) were observed for **3** with the frequency of 1−1488.1 Hz at 1.8 K using an applied magnetic field in the range of 0−2500 Oe (Figure S19 in the Supporting Information), suggesting that **3** does not exhibit SMM properties.

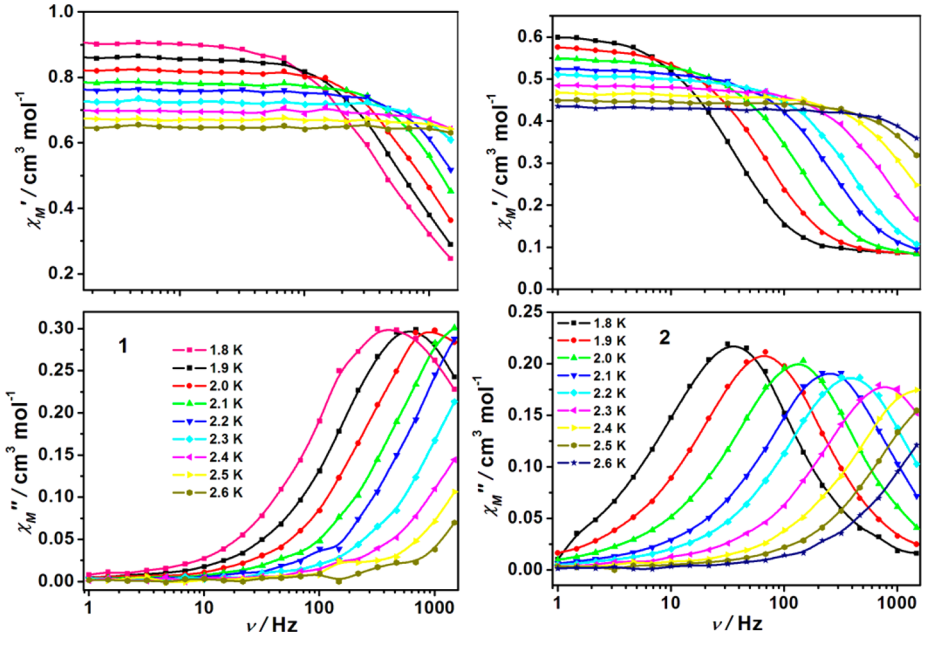

Figure 9. Frequency dependence of the ac susceptibility from 1.8 to 2.6 K under a 600 Oe dc field for **1** and **2**. The solid lines are guides for the eye.

DOI: 10.1021/acs.inorgchem.6b01544
Inorg. Chem. 2016, 55, 12603−12617

The Cole−Cole plots were generated from the ac magnetic susceptibilities of **1** and **2** (Figures S18 and S19 in the Supporting Information) and fitted using the generalized Debye model (eq 3):[47]

$$\chi_{ac}(\omega) = \chi_S + \frac{\chi_T - \chi_S}{1 + (i\omega\tau)^{(1-\alpha)}} \quad (3)$$

where χ_T and χ_S are the isothermal and adiabatic susceptibilities, respectively, ω is the angular frequency, τ is the relaxation time, and α indicates deviation from a pure Debye model. The fitting parameters are summarized in Table S7 in the Supporting Information. The obtained α values for **1** and **2** are found within the ranges of 0.03−0.17 and 0.1−0.12, respectively, suggesting the occurrence of a single relaxation process.

The relaxation times extracted from the Debye model were fit by the Arrhenius law $\tau = \tau_0 \exp(U_{eff}/kT)$ to give U_{eff} = 12 cm^{-1} ($\tau_0 = 4.14 \times 10^{-8}$ s) for **1** and U_{eff} = 20 cm^{-1} ($\tau_0 = 2.1 \times 10^{-9}$ s) for **2**, respectively (Figure S22 in the Supporting Information). Such a derivation of the effective energy barrier is based on the assumption that the thermally activated Orbach process is the dominant relaxation mechanism in the studied temperature range. However, these energy barriers obtained by alternating-current (ac) susceptibility measurements are much smaller than the ZFS energy difference between the ground and excited states accurately determined from INS studies (22.5(2) and 26.6(3) cm^{-1} for **1** and **2**, respectively). This suggests that the results obtained by alternating-current (ac) susceptibility measurements underestimate the energy barriers and other mechanisms such as Raman processes may occur in the magnetic relaxation of **1** and **2**. Several detailed studies show that a Raman mechanism makes significant contributions to the relaxation process for Co(II)-based SIMs with easy-plane magnetic anisotropy.[16a,d,e,17a,c] On these grounds, we tentatively model the contribution to the relaxation rate in **1** and **2** by using eq 4:[48]

$$\tau^{-1} = CT^n + \tau_0^{-1} \exp(-U_{eff}/kT) \quad (4)$$

where the first term in eq 4 represents the contribution of the Raman or Raman-like process. The second term is for the Orbach process. As presented above, the energy barriers U_{eff} of the Orbach process were determined to be 22.5 for **1** and 26.6 cm^{-1} for **2** by INS studies. Therefore, the U_{eff} values were fixed in this fit. The best fit of the relaxation time vs temperature curves gives the following parameters: C = 128.2, n = 5, $\tau_0 = 6.5 \times 10^{-11}$ s, U_{eff} = 22.5 cm^{-1} (fixed) for **1**; C = 0.94, n = 9, $\tau_0 = 1.9 \times 10^{-11}$ s, U_{eff} = 26.6 cm^{-1} (fixed) for **2**. The fit reproduces the experimental data very well (Figure 10). It can be concluded that the contribution of the Orbach process in **1** is very small in comparison with the Raman process. Furthermore, if the Orbach process is neglected, the relaxation time data can be fit by the power law $\tau^{-1} = CT^n$ with the resulting values C = 16.4 and n = 8.6 (Figure S23 in the Supporting Information). These fits suggest that the optical acoustic Raman-like mechanism is the dominant process in the magnetic relaxation of **1**. In the case of **2**, the Raman process dominates in the low-temperature region whereas the relaxation process in the high-temperature range is attributed to the Orbach mechanism.

Our INS spectra showed the presence of a phonon peak around 18 cm^{-1} in **1** (Figure 3), which is absent in the INS spectra of **2** (Figure 5). In each unit cell (2479.1(8) Å^3) of complex **1**, containing two molecules each of $(PPh_4)_2[Co(NO_3)_4]$ and CH_2Cl_2, there is a total of 224 atoms. In comparison, in each unit cell of **2**, containing two molecules of $(MePPh_3)_2[Co(NO_3)_4]$, there is a total of 186 atoms, a reflection of the smaller cation and the lack of CH_2Cl_2 in the cell. Since phonon modes are lattice and intramolecular vibrations,[49] the larger number of atoms in the unit cell of **1** is expected to lead to more low-energy delocalized vibrations in its INS spectra.[50] The absence of phonon peaks in the same region in the INS spectra of **2** (Figure 5) is perhaps a result of a smaller number of atoms in its unit cell. There could be few phonons of appropriate frequency to promote a more efficient relaxation in **2**. The phonon peak around 18 cm^{-1} in **1**, which is fairly low in energy, could be involved in the Raman-type relaxation in **1**, leading to its faster magnetic relaxation in comparison to that in **2**, as observed in the ac susceptibility studies. Carretta and co-workers have observed that low-energy optical phonon modes in Fe_8 enhance its magnetic relaxation process.[51]

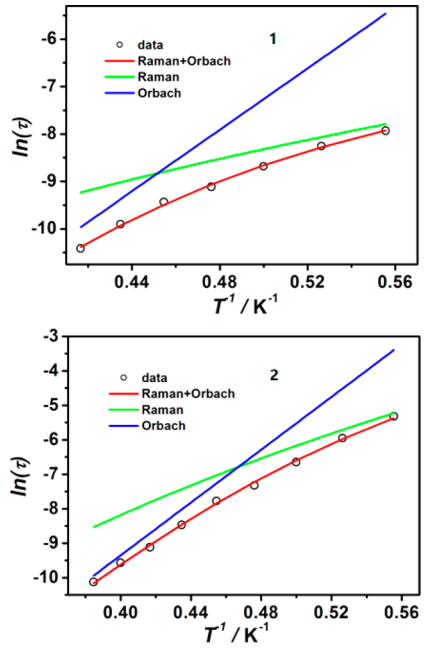

Figure 10. Temperature dependence of the magnetization relaxation rates of **1** and **2** under an applied dc field of 0.6 kOe. The solid red lines represent the best fit by using eq 4. The other solid lines represent data fits using individual Raman (green) and Orbach (blue) processes, respectively.

It is also worth noting that, in addition to giving the ZFS transitions, INS, a spectroscopic method, also directly shows phonon modes in the samples. Unlike electromagnetic IR and Raman spectroscopy with selection rules for vibrational peaks, there is no selection rule for the vibrational peaks in INS spectroscopy, which is based on the kinetic energy transfer between incident neutrons and the samples. Additional studies linking the INS spectra to the ac susceptibility data to understand relaxation mechanisms are needed.

Theoretical Investigations. Complete active space second-order perturbation theory (CASPT2) considering the effect of the dynamic electronic correlation on the basis of complete active space self-consistent field (CASSCF) with the MOLCAS 8.0 program package[29] were performed on the complete structures of three complexes (see Computational Details). Tables S8 and S9 in the Supporting Information show that the energy differences between the lowest two spin-free

DOI: 10.1021/acs.inorgchem.6b01544
Inorg. Chem. 2016, 55, 12603−12617

states for **1**−**3** are much larger than those between the lowest two spin−orbit states. Thus, we can use the ZFS parameters D and E to depict their magnetic anisotropies. The calculated D and E values (cm^{-1}) and **g** values (x, y, z) of the three complexes are given in Table 3, where all the calculated D values of three complexes are positive, and they are all close to the experimental values determined by INS/HE-FPR data. The calculated orientations of g_x, g_y, and g_z (hard axis) on the Co^{II} ion of **1**−**3** are shown in Figure S24 in the Supporting Information. The calculated $\chi_M T$ versus T plots of **1**−**3** are shown in Figure S25 in the Supporting Information, which are comparable to the experimental curves.[14b]

Table 3. Calculated D and E Values and g Tensors of Complexes 1−3 using CASPT2 with MOLCAS 8.0

	1	2	3
D, cm^{-1}	11.3	23.1	7.7
E, cm^{-1}	−0.4	−0.9	0.3
g_x, cm^{-1}	2.499	2.501	2.300
g_y, cm^{-1}	2.443	2.261	2.296
g_z, cm^{-1}	2.174	2.239	2.216

To deeply analyze the magnetic anisotropyies of **1**−**3**, ORCA 3.03 calculations[30] were performed with the n-electron valence state perturbation theory (NEVPT2)[31] method (see Computational Details). The effective Hamiltonian implemented in ORCA was used to extract the ZFS parameters D and E. The calculated D and E values of **1**−**3** and the important contributions of the excited states to the ZFS parameters are shown in Table 4.

The calculated D values of **1**−**3** using NEVPT2 have some differences from those calculated using CASPT2 and the values determined by INS/HFEPR, but they have the same trends (D(**2**) > D(**1**) > D(**3**)). From observation of the output of the NEVPT2 calculations, only the lowest three or four excited states play an important role in the sign and magnitude of the D and E values for **1**−**3**. Since the spin−spin coupling has a smaller contribution to the magnetic anisotropy, we only use the spin−orbit operator to analyze the sign and magnitude of D. Table 4 indicates that the first quartet excited state has a larger contribution to the total D for **1**−**3**, and the total contributions from the other three excited states are almost close to 0 except for **2**. It is also found that the first excited state contribution for **2** is the smallest, but the total D value of **2** is the largest. Thus, the positive contributions from the higher excited states other than the lowest four states of **2** are the largest, which makes it have the largest positive D value. Moreover, as we can see in Figure S26 in the Supporting Information, the lowest three or four spin-free excited states (first, second, third, or fourth quartets) are very multiconfigurational, which prevents us from further rationalizing the contributions of the excited states to the total D value only using the 3d orbitals.

CONCLUSIONS

Utilizing three different countercations (Ph_4P^+, $MePh_3P^+$, Ph_4As^+), three high-coordinate Co(II) complexes containing $[Co(NO_3)_4]^{2-}$ anions have been prepared. **1** and **2** with Ph_4P^+ and $MePh_3P^+$ show an irregular seven-coordinate geometry. The X-ray redetermination for **3** confirms its distorted-dodecahedral configuration, in which two nitrate groups are disordered. The magnetization, INS, and HF-EPR studies reveal the easy-plane magnetic anisotropy for **1**−**3** (D > 0). Slow magnetic relaxations were observed for **1** and **2** under a dc field of 600 Oe, while no similar behavior was found in **3**. Such fine tuning of the magnetic properties of SIMs by counterions have been rarely reported in SMMs based on transition-metal ions[16k,l,52] and lanthanide ions.[53] These studies provide a new example of modulating the properties of SIMs by varying the counterions.

ASSOCIATED CONTENT

Supporting Information

The Supporting Information is available free of charge on the ACS Publications website at DOI: 10.1021/acs.inorgchem.6b01544.

Summary of crystal data and refinement details for **1**−**3**, calculations by SHAPE, fitting data for the Cole−Cole plot, additional figures for magnetic characterization, treatment of INS data, additional INS figures, and results of the theoretical calculations (PDF)
Additional structural data for **1** (CIF)
Additional structural data for **2** (CIF)
Additional structural data for **3** (CIF)

AUTHOR INFORMATION

Corresponding Authors

*E-mail for Y.-Q.Z.: zhangyiquan@njnu.edu.cn.
*E-mail for X.-T.C.: xtchen@netra.nju.edu.cn.
*E-mail for Z.W.: zxwang@hust.edu.cn.
*E-mail for A.A.P.: podlesnyakaa@ornl.gov.
*E-mail for Z.-L.X.: xue@utk.edu.

ORCID

Xue-Tai Chen: 0000-0001-5518-5557

Notes

The authors declare no competing financial interest.

ACKNOWLEDGMENTS

We are grateful for financial support from the National Basic Research Program of China (No. 2013CB922102 to X.-T.C.

Table 4. Calculated D and E Values (cm^{-1}) of 1−3 and Main Perturbative Contributions of the Quartet Excited States to D and E using NEVPT2 with ORCA 3.03

	1		2		3	
	D (cm^{-1})	E (cm^{-1})	D (cm^{-1})	E (cm^{-1})	D (cm^{-1})	E (cm^{-1})
total	17.4	3.4	19.0	5.7	15.0	2.9
first quartet	19.5	19.9	12.6	10.8	15.4	15.4
second quartet	15.2	−15.2	−5.0	−1.0	11.7	−11.7
third quartet	−14.7	−0.1	4.6	−1.8		
fourth quartet			3.2	−0.9	−10.5	0.0

DOI: 10.1021/acs.inorgchem.6b01544
Inorg. Chem. 2016, 55, 12603−12617

and Y.S.), the Natural Science Grant of China (No. 21471078 to X.-T.C.), the Natural Science Foundation of Jiangsu Province of China (BK20151542), and the U.S. National Science Foundation (CHE-1362548 and CHE-1633870 to Z.-L.X.). Acknowledgment is also made to the donors of the American Chemical Society Petroleum Research Fund for partial support of this research. The research at ORNL's Spallation Neutron Source was sponsored by the Scientific User Facilities Division, Office of Basic Energy Sciences, U.S. Department of Energy.

REFERENCES

(1) (a) Gatteschi, D.; Sessoli, R.; Villain, J. *Molecular Nanomagnets*; Oxford University Press: Oxford, U.K., 2006. (b) Winpenny, R. E. P. *Single-Molecule Magnets and Related Phenomena*; Springer-Verlag: Berlin, 2006. (c) Winpenny, R. E. P. *Molecular Cluster Magnets*; World Scientific: Singapore, 2012. (d) Gao, S. *Molecular Nanomagnets and and Related Phenomena*; Springer-Verlag: Berlin, 2015.

(2) (a) Christou, G. Single-molecule magnets: a molecular approach to nanoscale magnetic materials. *Polyhedron* **2005**, *24*, 2065−2075. (b) Bagai, R.; Christou, G. The Drosophila of single-molecule $[Mn_{12}O_{12}(O_2CR)_{16}(H_2O)_4]$. *Chem. Soc. Rev.* **2009**, *38*, 1011−1026. (c) Gatteschi, D.; Sessoli, R.; Cornia, A. Single-molecule magnets based on iron(III) oxo clusters. *Chem. Commun.* **2000**, *9*, 725−732. (d) Pedersen, K. S.; Bendix, J.; Clérac, R. Single-molecule magnet engineering: building-block approach. *Chem. Commun.* **2014**, *50*, 4396−4415.

(3) (a) Gatteschi, D.; Sessoli, R. Quantum Tunneling of Magnetization and Related Phenomena in Molecular Materials. *Angew. Chem., Int. Ed.* **2003**, *42*, 268−297. (b) Wernsdorfer, W.; Sessoli, R. Quantum Phase Interference and Parity Effects in Magnetic Molecular Clusters. *Science* **1999**, *284*, 133−135. (c) Leuenberger, M. N.; Loss, D. Quantum computing in molecular magnets. *Nature* **2001**, *410*, 789−793. (d) Bogani, L.; Wernsdorfer, W. Molecular spintronics using single-molecule magnets. *Nat. Mater.* **2008**, *7*, 179−186.

(4) (a) Waldmann, O. A Criterion for the Anisotropy Barrier in Single-Molecule Magnets. *Inorg. Chem.* **2007**, *46*, 10035−10037. (b) Neese, F.; Pantazis, D. A. What is not required to make a single molecule magnet. *Faraday Discuss.* **2011**, *148*, 229−238.

(5) (a) Ako, A. M.; Hewitt, I. J.; Mereacre, V.; Clérac, R.; Wernsdorfer, W.; Anson, C. E.; Powell, A. K. A Ferromagnetically Coupled Mn_{19} Aggregate with a Record $S = 83/2$ Ground Spin State. *Angew. Chem., Int. Ed.* **2006**, *45*, 4926−4929. (b) Kang, S.; Zheng, H.; Liu, T.; Hamachi, K.; Kanegawa, S.; Sugimoto, K.; Shiota, Y.; Hayami, S.; Mito, M.; Nakamura, T.; Nakano, M.; Baker, M. L.; Nojiri, H.; Yoshizawa, K.; Duan, C.; Sato, O. A ferromagnetically coupled Fe_{42} cyanide-bridged nanocage. *Nat. Commun.* **2015**, *6*, 5955.

(6) (a) Woodruff, D. N.; Winpenny, R. E. P.; Layfield, R. A. Lanthanide Single-Molecule Magnets. *Chem. Rev.* **2013**, *113*, 5110−5148. (b) Feltham, H. L. C.; Brooker, S. Review of purely 4f and mixed-metal nd-4f single-molecule magnets containing only one lanthanide ion. *Coord. Chem. Rev.* **2014**, *276*, 1−33.

(7) Reviews and highlights on 3d-ion SIMs: (a) Craig, G. A.; Murrie, M. 3d single-ion magnets. *Chem. Soc. Rev.* **2015**, *44*, 2135−2147. (b) Dey, M.; Gogoi, N. Geometry-Mediated Enhancement of Single-Ion Anisotropy: A Route to Single-Molecule Magnets with a High Blocking Temperature. *Angew. Chem., Int. Ed.* **2013**, *52*, 12780−12782. (c) Bar, A. K.; Pichon, C.; Sutter, J.-P. Magnetic anisotropy in two- to eight-coordinated transition−metal complexes: Recent developments in molecular magnetism. *Coord. Chem. Rev.* **2016**, *308*, 346−380. (d) Frost, J. M.; Harriman, K. L. M.; Murugesu, M. The rise of 3-d single-ion magnets in molecular magnetism: towards materials from molecules? *Chem. Sci.* **2016**, *7*, 2470−2491. (e) Atanasov, M.; Aravena, D.; Suturina, E.; Bill, E.; Maganas, D.; Neese, F. First principles approach to the electronic structure, magnetic anisotropy and spin relaxation in mononuclear 3d-transition metal single molecule magnets. *Coord. Chem. Rev.* **2015**, *289−290*, 177−214. (f) Gómez-Coca, S.; Aravena, D.; Morales, R.; Ruiz, E. Large magnetic anisotropy in mononuclear metal complexes. *Coord. Chem. Rev.* **2015**, *289−290*, 379−392.

(8) Cornia, A.; Rigamonti, L.; Boccedi, S.; Clérac, R.; Rouzières, M.; Sorace, L. Magnetic blocking in extended metal atom chains: a pentachromium(II) complex behaving as a single-molecule magnet. *Chem. Commun.* **2014**, *50*, 15191−15194.

(9) (a) Ishikawa, R.; Miyamoto, R.; Nojiri, H.; Breedlove, B. K.; Yamashita, M. Slow Relaxation of the Magnetization of an Mn^{III} Single Ion. *Inorg. Chem.* **2013**, *52*, 8300−8302. (b) Grigoropoulos, A.; Pissas, M.; Papatolis, P.; Psycharis, V.; Kyritsis, P.; Sanakis, Y. Spin-Relaxation Properties of a High-Spin Mononuclear $Mn^{III}O_6$-Containing Complex. *Inorg. Chem.* **2013**, *52*, 12869−12871. (c) Vallejo, J.; Pascual-Álvarez, A.; Cano, J.; Castro, I.; Julve, M.; Lloret, F.; Krzystek, J.; De Munno, G.; Armentano, D.; Wernsdorfer, W.; Ruiz-García, R.; Pardo, E. Field-Induced Hysteresis and Quantum Tunneling of the Magnetization in a Mononuclear Manganese(III) Complex. *Angew. Chem., Int. Ed.* **2013**, *52*, 14075−14079. (d) Chen, L.; Wang, J.; Liu, Y.-Z.; Song, Y.; Chen, X.-T.; Zhang, Y.-Q.; Xue, Z.-L. Slow Magnetic Relaxation in Mononuclear Octahedral Manganese(III) Complexes with Dibenzoylmethanide Ligands. *Eur. J. Inorg. Chem.* **2015**, *2015*, 271−278. (e) Pascual-Alvarez, A.; Vallejo, J.; Pardo, E.; Julve, M.; Lloret, F.; Krzystek, J.; Armentano, D.; Wernsdorfer, W.; Cano, J. Field-Induced Slow Magnetic Relaxation in a Mononuclear Manganese(III)−Porphyrin Complex. *Chem. - Eur. J.* **2015**, *21*, 17299−17307.

(10) For Fe-SIMs, see for examples: (a) Freedman, D. E.; Harman, W. H.; Harris, T. D.; Long, G. J.; Chang, C. J.; Long, J. R. Slow Magnetic Relaxation in a High-Spin Iron(II) Complex. *J. Am. Chem. Soc.* **2010**, *132*, 1224−1225. (b) Harman, W. H.; Harris, T. D.; Freedman, D. E.; Fong, H.; Chang, A.; Rinehart, J. D.; Ozarowski, A.; Sougrati, M. T.; Grandjean, F.; Long, G. J.; Long, J. R.; Chang, C. J. Slow Magnetic Relaxation in a Family of Trigonal Pyramidal Iron(II) Pyrrolide Complexes. *J. Am. Chem. Soc.* **2010**, *132*, 18115−18126. (c) Zadrozny, J. M.; Xiao, D. J.; Atanasov, M.; Long, G. J.; Grandjean, F.; Neese, F.; Long, J. R. Magnetic blocking in a linear iron(I) complex. *Nat. Chem.* **2013**, *5*, 577−581. (d) Samuel, P. P.; Mondal, K. C.; Sk, N. A.; Roesky, H. W.; Carl, E.; Neufeld, R.; Stalke, D.; Demeshko, S.; Meyer, F.; Ungur, L.; Chibotaru, L. F.; Christian, J.; Ramachandran, V.; van Tol, J.; Dalal, N. S. Electronic Structure and Slow Magnetic Relaxation of Low-Coordinate Cyclic Alkyl(amino) Carbene Stabilized Iron(I) Complexes. *J. Am. Chem. Soc.* **2014**, *136*, 11964−11971. (e) Zadrozny, J. M.; Atanasov, M.; Bryan, A. M.; Lin, C. Y.; Rekken, B. D.; Power, P. P.; Neese, F.; Long, J. R. Slow magnetization dynamics in a series of two coordinate iron(II) complexes. *Chem. Sci.* **2013**, *4*, 125−138. (f) Lin, P. - H.; Smythe, N. C.; Gorelsky, S. I.; Maguire, S.; Henson, N. J.; Korobkov, I.; Scott, B. L.; Gordon, J. C.; Baker, R. T.; Murugesu, M. Importance of Out-of-State Spin-Orbit Coupling for Slow Magnetic Relaxation in Mononuclear Fe^{II} Complexes. *J. Am. Chem. Soc.* **2011**, *133*, 15806−15809. (g) Feng, X.; Mathonière, C.; Jeon, I.-R.; Rouzières, M.; Ozarowski, A.; Aubrey, M. L.; Gonzalez, M. I.; Clèrac, R.; Long, J. R. Tristability in a Light-Actuated Single-Molecule Magnet. *J. Am. Chem. Soc.* **2013**, *135*, 15880−15884. (h) Bar, A. K.; Pichon, C.; Gogoi, N.; Duhayon, C.; Ramasesha, S.; Sutter, J.-P. Single-ion magnet behaviour of heptacoordinated Fe(II) complexes: on the importance of supramolecular organization. *Chem. Commun.* **2015**, *51*, 3616−3619. (i) Shao, D.; Zhao, X.-H.; Zhang, S.-L.; Wu, D.-Q.; Wei, X.-Q.; Wang, X.-Y. Structural and magnetic tuning from a field-induced single-ion magnet to a single-chain magnet by anions. *Inorg. Chem. Front.* **2015**, *2*, 846−853. (j) Mossin, S.; Tran, B. L.; Adhikari, D.; Pink, M.; Heinemann, F. W.; Sutter, J.; Szilagyi, R. K.; Meyer, K.; Mindiola, D. J. A Mononuclear Fe(III) Single Molecule Magnet with a $3/2 \leftrightarrow 5/2$ Spin Crossover. *J. Am. Chem. Soc.* **2012**, *134*, 13651−13661. (k) Sato, R.; Suzuki, K.; Minato, T.; Shinoe, M.; Yamaguchi, K.; Mizuno, N. Field-induced slow magnetic relaxation of octahedrally coordinated mononuclear Fe(III)-, Co(II)-, and Mn(III)-containing polyoxometalates. *Chem. Commun.* **2015**, *51*, 4081−4084.

(11) (a) Poulten, R. C.; Page, M. J.; Algarra, A. G.; Le Roy, J. J.; Lòpez, I.; Carter, E.; Llobet, A.; Macgregor, S. A.; Mahon, M. F.; Murphy, D. M.; Murugesu, M.; Whittlesey, M. K. Synthesis, Electronic

DOI: 10.1021/acs.inorgchem.6b01544
Inorg. Chem. 2016, 55, 12603−12617

Structure, and Magnetism of $[Ni(6\text{-}Mes)_2]^+$: A Two-Coordinate Nickel(I) Complex Stabilized by Bulky N-Heterocyclic Carbenes. *J. Am. Chem. Soc.* **2013**, *135*, 13640−13643. (b) Lin, W.; Bodenstein, T.; Mereacre, V.; Fink, K.; Eichhöfer, A. Field-Induced Slow Magnetic Relaxation in the Ni(I) Complexes $[NiCl(PPh_3)_2]\cdot C_4H_8O$ and $[Ni(N(SiMe_3)_2)(PPh_3)_2]$. *Inorg. Chem.* **2016**, *55*, 2091−2100. (c) Miklovič, J.; Valigura, D.; Boča, R.; Titiš, J. A mononuclear Ni(II) complex: a field induced single-molecule magnet showing two slow relaxation processes. *Dalton Trans.* **2015**, *44*, 12484−12487. (d) Marriott, K. E. R.; Bhaskaran, L.; Wilson, C.; Medarde, M.; Ochsenbein, S. T.; Hill, S.; Murrie, M. Pushing the limits of magnetic anisotropy in trigonal bipyramidal Ni(II). *Chem. Sci.* **2015**, *6*, 6823−6828.

(12) (a) Martinez-Lillo, J.; Mastropietro, T. F.; Lhotel, E.; Paulsen, C.; Cano, J.; De Munno, G.; Faus, J.; Lloret, F.; Julve, M.; Nellutla, S.; Krzystek, J. Highly Anisotropic Rhenium(IV) Complexes: New Examples of Mononuclear Single-Molecule Magnets. *J. Am. Chem. Soc.* **2013**, *135*, 13737−13748. (b) Pedersen, K. S.; Sigrist, M.; Soensen, M. A.; Barra, A.-L.; Weyhermuller, T.; Piligkos, S.; Thuesen, C. A.; Vinum, M. G.; Mutka, H.; Weihe, H.; Clérac, R.; Bendix, J. A Robust Module for the Design of Molecule-Based Magnetic Materials. *Angew. Chem., Int. Ed.* **2014**, *53*, 1351−1354.

(13) Eichhofer, A.; Lan, Y.; Mereacre, V.; Bodenstein, T.; Weigend, F. Slow Magnetic Relaxation in Trigonal-Planar Mononuclear Fe(II) and Co(II) Bis(trimethylsilyl)amido Complexes−A Comparative Study. *Inorg. Chem.* **2014**, *53*, 1962−1974.

(14) (a) Zadrozny, J. M.; Liu, J. J.; Piro, N. A.; Chang, C. J.; Hill, S.; Long, J. R. Slow magnetic relaxation in a pseudotetrahedral cobalt(II) complex with easy-plane anisotropy. *Chem. Commun.* **2012**, *48*, 3927−3929. (b) Gomez-Coca, S.; Cremades, E.; Aliaga-Alcalde, N.; Ruiz, E. Mononuclear Single-Molecule Magnets: Tailoring the Magnetic Anisotropy of First-Row Transition-Metal Complexes. *J. Am. Chem. Soc.* **2013**, *135*, 7010−7018. (c) Huang, W.; Liu, T.; Wu, D. Y.; Cheng, J. J.; Ouyang, Z. W.; Duan, C. Y. Field-induced slow relaxation of magnetization in a tetrahedral Co(II) complex with easy plane anisotropy. *Dalton Trans.* **2013**, *42*, 15326−15331. (d) Vaidya, S.; Upadhyay, A.; Singh, S. K.; Gupta, T.; Tewary, S.; Langley, S. K.; Walsh, J. P. S.; Murray, K. S.; Rajaraman, G.; Shanmugam, M. A synthetic strategy for switching the single ion anisotropy in tetrahedral Co(II) complexes. *Chem. Commun.* **2015**, *51*, 3739−3742. (e) Smolko, L.; Černák, J.; Dušek, M.; Miklovič, J.; Titiš, J.; Boča, R. Three tetracoordinate Co(II) complexes $[Co(biq)X_2]$ (X = Cl, Br, I) with easy-plane magnetic anisotropy as field-induced single-molecule magnets. *Dalton Trans.* **2015**, *44*, 17565−17571. (f) Zadrozny, J. M.; Long, J. R. Slow Magnetic Relaxation at Zero Field in the Tetrahedral Complex $[Co(SPh)_4]^{2-}$. *J. Am. Chem. Soc.* **2011**, *133*, 20732−20734. (g) Zadrozny, J. M.; Telser, J.; Long, J. R. Slow magnetic relaxation in the tetrahedral cobalt(II) complexes $[Co(EPh)_4]^{2-}$ (E = O, S, Se). *Polyhedron* **2013**, *64*, 209−217. (h) Cao, D. K.; Feng, J. Q.; Ren, M.; Gu, Y. W.; Song, Y.; Ward, M. D. A mononuclear cobalt(II)−dithienylethene complex showing slow magnetic relaxation and photochromic behavior. *Chem. Commun.* **2013**, *49*, 8863−8865. (i) Buchholz, A.; Eseola, A. O.; Plass, W. Slow magnetic relaxation in mononuclear tetrahedral cobalt(II) complexes with 2-(1H-imidazol-2-yl)phenol based ligands. *C. R. Chim.* **2012**, *15*, 929−936. (j) Yang, F.; Zhou, Q.; Zhang, Y. Q.; Zeng, G.; Li, G. H.; Shi, Z.; Wang, B. W.; Feng, S. H. Inspiration from old molecules: field-induced slow magnetic relaxation in three air-stable tetrahedral cobalt(II) compounds. *Chem. Commun.* **2013**, *49*, 5289−5291. (k) Fataftah, M. S.; Zadrozny, J. M.; Rogers, D. M.; Freedman, D. E. A Mononuclear Transition Metal Single-Molecule Magnet in a Nuclear Spin-Free Ligand Environment. *Inorg. Chem.* **2014**, *53*, 10716−10721. (l) Cucos, P.; Tuna, F.; Sorace, L.; Matei, I.; Maxim, C.; Shova, S.; Gheorghe, R.; Caneschi, A.; Hillebrand, M.; Andruh, M. Magnetic and Luminescent Binuclear Double-Stranded Helicates. *Inorg. Chem.* **2014**, *53*, 7738−7747. (m) Boča, R.; Miklovič, J.; Titiš, J. Simple Mononuclear Cobalt(II) Complex: A Single-Molecule Magnet Showing Two Slow Relaxation Processes. *Inorg. Chem.* **2014**, *53*, 2367−2369. (n) Carl, E.; Demeshko, S.; Meyer, F.; Stalke, D. Triimidosulfonates as Acute Bite-Angle Chelates: Slow Relaxation of the Magnetization in Zero Field and Hysteresis Loop of a Co^{II} Complex. *Chem. - Eur. J.* **2015**, *21*, 10109−10115. (o) Cao, D.-K.; Wei, R.-H.; Li, X.-X.; Gu, Y.-W. Multifunctional mononuclear bisthienylethenecobalt(II) complexes: structures, slow magnetic relaxation and photochromic behavior. *Dalton Trans.* **2015**, *44*, 5755−5762. (p) Saber, M. R.; Dunbar, K. R. *Chem. Commun.* **2014**, *50*, 12266. (q) Rechkemmer, Y.; Breitgoff, F. D.; van der Meer, M.; Atanasov, M.; Hakl, M.; Orlita, M.; Neugebauer, P.; Neese, F.; Sarkar, B.; van Slageren, J. A four-coordinate cobalt(II) single-ion magnet with coercivity and a very high energy barrier. *Nat. Commun.* **2016**, *7*, 10467.

(15) (a) Jurca, T.; Farghal, A.; Lin, P.-H.; Korobkov, I.; Murugesu, M.; Richeson, D. S. Single-Molecule Magnet Behavior with a Single Metal Center Enhanced through Peripheral Ligand Modifications. *J. Am. Chem. Soc.* **2011**, *133*, 15814−15817. (b) Habib, F.; Luca, O. R.; Vieru, V.; Shiddiq, M.; Korobkov, I.; Gorelsky, S. I.; Takase, M. K.; Chibotaru, L. F.; Hill, S.; Crabtree, R. H.; Murugesu, M. Influence of the Ligand Field on Slow Magnetization Relaxation versus Spin Crossover in Mononuclear Cobalt Complexes. *Angew. Chem., Int. Ed.* **2013**, *52*, 11290−11293. (c) Ruamps, R.; Batchelor, L. J.; Guillot, R.; Zakhia, G.; Barra, A.-L.; Wernsdorfer, W.; Guihéry, N.; Mallah, T. Ising-type magnetic anisotropy and single molecule magnet behaviour in mononuclear trigonal bipyramidal Co(II) complexes. *Chem. Sci.* **2014**, *5*, 3418−3424. (d) Piñero Cruz, D. M.; Woodruff, D. N.; Jeon, I.-R.; Bhowmick, I.; Secu, M.; Hillard, E. A.; Dechambenoit, P.; Clérac, R. Switching off the single-molecule magnet properties of the $[Co^{II}(Me_6tren)(OH_2)]^{2+}$ module by complexation with *trans*-$[Ru^{III}(salen)(CN)_2]^-$. *New J. Chem.* **2014**, *38*, 3443−3448. (e) Schweinfurth, D.; Sommer, M. G.; Atanasov, M.; Demeshko, S.; Hohloch, S.; Meyer, F.; Neese, F.; Sarkar, B. The Ligand Field of the Azido Ligand: Insights into Bonding Parameters and Magnetic Anisotropy in a Co(II)−Azido Complex. *J. Am. Chem. Soc.* **2015**, *137*, 1993−2005. (f) Shao, F.; Cahier, B.; Guihéry, N.; Riviére, E.; Guillot, R.; Barra, A.-L.; Lan, Y.; Wernsdorfer, W.; Campbell, V. E.; Mallah, T. Tuning the Ising-type anisotropy in trigonal bipyramidal Co(II) complexes. *Chem. Commun.* **2015**, *51*, 16475−16478. (g) Rajnák, C.; Titiš, J.; Fuhr, O.; Ruben, M.; Boča, R. Single-Molecule Magnetism in a Pentacoordinate Cobalt(II) Complex Supported by an Antenna Ligand. *Inorg. Chem.* **2014**, *53*, 8200−8202.

(16) (a) Colacio, E.; Ruiz, J.; Ruiz, E.; Cremades, E.; Krzystek, J.; Carretta, S.; Cano, J.; Guidi, T.; Wernsdorfer, W.; Brechin, E. K. Slow Magnetic Relaxation in a Co^{II}-Y^{III} Single-Ion Magnet with Positive Axial Zero-Field Splitting. *Angew. Chem., Int. Ed.* **2013**, *52*, 9130−9134. (b) Vallejo, J.; Castro, I.; Ruiz-García, R.; Cano, J.; Julve, M.; Lloret, F.; De Munno, G.; Wernsdorfer, W.; Pardo, W. E. Field-Induced Slow Magnetic Relaxation in a Six-Coordinate Mononuclear Cobalt(II) Complex with a Positive Anisotropy. *J. Am. Chem. Soc.* **2012**, *134*, 15704−15707. (c) Wu, D. Y.; Zhang, X. X.; Huang, P.; Huang, W.; Ruan, M. Y.; Ouyang, Z. W. Tuning Transverse Anisotropy in Co^{III}−Co^{II}−Co^{III} Mixed-Valence Complex toward Slow Magnetic Relaxation. *Inorg. Chem.* **2013**, *52*, 10976−10982. (d) Gómez-Coca, S.; Urtizberea, A.; Cremades, E.; Alonso, P. J.; Camón, A.; Ruiz, E.; Luis, F. Origin of slow magnetic relaxation in Kramers ions with non-uniaxial anisotropy. *Nat. Commun.* **2014**, *5*, 4300. (e) Ishikawa, R.; Horii, Y.; Nakanishi, R.; Ueno, S.; Breedlove, B. K.; Yamashita, M.; Kawata, S. Field-Induced Single-Ion Magnetism Based on Spin-Phonon Relaxation in a Distorted Octahedral High-Spin Cobalt(II) Complex. *Eur. J. Inorg. Chem.* **2016**, *2016*, 3233−3239. (f) Zhu, Y.-Y.; Zhu, M.-S.; Yin, T.-T.; Meng, Y.-S.; Wu, Z.-Q.; Zhang, Y.-Q.; Gao, S. Cobalt(II) Coordination Polymer Exhibiting Single-Ion-Magnet-Type Field-Induced Slow Relaxation Behavior. *Inorg. Chem.* **2015**, *54*, 3716−3718. (g) Zhu, Y.-Y.; Cui, C.; Zhang, Y.-Q.; Jia, J.-H.; Guo, X.; Gao, C.; Qian, K.; Jiang, S.-D.; Wang, B.-W.; Wang, Z.-M.; Gao, S. Zero-field slow magnetic relaxation from single Co(II) ion: a transition metal single-molecule magnet with high anisotropy barrier. *Chem. Sci.* **2013**, *4*, 1802−1806. (h) Chandrasekhar, V.; Dey, A.; Mota, A. J.; Colacio, E. Slow Magnetic Relaxation in Co(III)−Co(II) Mixed-Valence Dinuclear Complexes with a $Co^{II}O_5X$ (X = Cl, Br, NO_3) Distorted-Octahedral Coordination Sphere. *Inorg. Chem.* **2013**, *52*, 4554−4561.

DOI: 10.1021/acs.inorgchem.6b01544
Inorg. Chem. 2016, 55, 12603−12617

(i) Plenk, C.; Krause, J.; Rentschler, E. A Click-Functionalized Single-Molecule Magnet Based on Cobalt(II) and Its Analogous Manganese-(II) and Zinc(II) Compounds. *Eur. J. Inorg. Chem.* **2015**, *2015*, 370−374. (j) Novikov, V. V.; Pavlov, A. A.; Nelyubina, Y. V.; Boulon, M.-E.; Varzatskii, O. A.; Voloshin, Y. Z.; Winpenny, R. E. P. A Trigonal Prismatic Mononuclear Cobalt(II) Complex Showing Single-Molecule Magnet Behavior. *J. Am. Chem. Soc.* **2015**, *137*, 9792−9795. (k) Zhu, Y.-Y.; Zhang, Y.-Q.; Yin, T.-T.; Gao, C.; Wang, B.-W.; Gao, S. A Family of $Co^{II}Co^{III}_3$ Single-Ion Magnets with Zero-Field Slow Magnetic Relaxation: Fine Tuning of Energy Barrier by Remote Substituent and Counter Cation. *Inorg. Chem.* **2015**, *54*, 5475−5486. (l) Zhang, Y.-Z.; Gómez-Coca, S.; Brown, A. J.; Saber, M. R.; Zhang, X.; Dunbar, K. R. Trigonal antiprismatic Co(II) single molecule magnets with large uniaxial anisotropies: importance of Raman and tunneling mechanisms. *Chem. Sci.* **2016**, *7*, 6519−6527.

(17) (a) Huang, X. C.; Zhou, C.; Shao, D.; Wang, X.-Y. Field-Induced Slow Magnetic Relaxation in Cobalt(II) Compounds with Pentagonal Bipyramid Geometry. *Inorg. Chem.* **2014**, *53*, 12671−12673. (b) Habib, F.; Korobkov, I.; Murugesu, M. Exposing the intermolecular nature of the second relaxation pathway in a mononuclear cobalt(II) single-molecule magnet with positive anisotropy. *Dalton Trans.* **2015**, *44*, 6368−6373. (c) Chen, L.; Chen, S.-Y.; Sun, Y.-C.; Guo, Y.-M.; Yu, L.; Chen, X.-T.; Wang, Z.; Ouyang, Z. W.; Song, Y.; Xue, Z.-L. Slow magnetic relaxation in mononuclear seven-coordinate cobalt(II) complexes with easy plane anisotropy. *Dalton Trans.* **2015**, *44*, 11482−11490.

(18) Chen, L.; Wang, J.; Wei, J.-M.; Wernsdorfer, W.; Chen, X.-T.; Zhang, Y.-Q.; Song, Y.; Xue, Z.-L. Slow Magnetic Relaxation in a Mononuclear Eight-Coordinate Cobalt(II) Complex. *J. Am. Chem. Soc.* **2014**, *136*, 12213−12216.

(19) (a) Cotton, F. A.; Bergman, J. G. Eight-Coordinate Complexes of Cobalt(II). A Principle Influencing the Occurrence of High Coordination Numbers. *J. Am. Chem. Soc.* **1964**, *86*, 2941−2942. (b) Bergman, J. G.; Cotton, F. A. The Crystal and Molecular Structure of Tetraphenylarsonium Tetranitratocobaltate(II); an Eight-Coordinate Cobalt(I1) Complex. *Inorg. Chem.* **1966**, *5*, 1208−1213. (c) Straub, D. K.; Drago, R. S.; Donoghue, J. T. Tetranitratometallates of Manganese(II), Cobalt(II), Nickel(II), and Copper(II). *Inorg. Chem.* **1962**, *1*, 848−852.

(20) (a) Morozov, I. V.; Fedorova, A. A.; Albov, D. V.; Kuznetsova, N. R.; Romanov, I. A.; Rybakov, V. B.; Troyanov, S. I. Synthesis and crystal structures of nitratocobaltates $Na_2[Co(NO_3)_4]$, $K_2[Co(NO_3)_4]$, and $Ag[Co(NO_3)_3]$ and potassium nitratonickelate $K_2[Ni(NO_3)_4]$. *Crystallogr. Rep.* **2008**, *53*, 237−245. (b) Morozov, I. V.; Kemnitz, E.; Troyanov, S. I. Synthesis and Crystal Structure of Cesium Nitratometalates(II), $Cs_2[M(NO_3)_4]$ (M = Mn, Co, Ni, Zn). *Z. Anorg. Allg. Chem.* **1999**, *625*, 1664−1669. (c) Tikhomirov, G. A.; Znamenkov, K. O.; Morozov, I. V.; Kemnitz, E.; Troyanov, S. I. Anhydrous nitrates and nitrosonium nitratometallates of manganese and cobalt, $M(NO_3)_2$, $NO[Mn(NO_3)_3]$, and $(NO)_2[Co(NO_3)_4]$: Synthesis and crystal structure. *Z. Anorg. Allg. Chem.* **2002**, *628*, 269−273.

(21) *SMART & SAINT Software Reference Manuals, version 6.45*; Bruker Analytical X-ray Systems: Madison, WI, 2003.

(22) Sheldrick, G. M. *SADABS: Software for Empirical Absorption Correction, version 2.05*; University of Göttingen, Göttingen, Germany, 2002.

(23) Sheldrick, G. M. *SHELXL97: Program for Crystal Structure Refinement*; University of Göttingen, Göttingen, Germany, 1997.

(24) Ehlers, G.; Podlesnyak, A.; Niedziela, J. L.; Iverson, E. B.; Sokol, P. E. The new cold neutron chopper spectrometer at the Spallation Neutron Source: design and performance. *Rev. Sci. Instrum.* **2011**, *82*, 085108.

(25) (a) Arnold, O.; Bilheux, J. C.; Borreguero, J. M.; Buts, A.; Campbell, S. I.; Chapon, L.; Doucet, M.; Drape, N.; Leal, R. F.; Gigg, M. A.; Lynch, V. E.; Markvardsen, A.; Mikkelson, D. J.; Mikkelson, R. L.; Miller, R.; Palmen, K.; Parker, P.; Passos, G.; Perring, T. G.; Peterson, P. F.; Ren, S.; Reuter, M. A.; Savici, A. T.; Taylor, J. W.; Taylor, R. J.; Tolchenov, R.; Zhou, W.; Zikovsky, J. Mantid—Data analysis and visualization package for neutron scattering and μ SR experiments. *Nucl. Instrum. Methods Phys. Res., Sect. A* **2014**, *764*, 156. (b) Azuah, R. T.; Kneller, L. R.; Qiu, Y.; Tregenna-Piggott, P. L. W.; Brown, C. M.; Copley, J. R. D.; Dimeo, R. M. DAVE: A Comprehensive Software Suite for the Reduction, Visualization, and Analysis of Low Energy Neutron Spectroscopic Data. *J. Res. Natl. Inst. Stand. Technol.* **2009**, *114*, 341.

(26) Basler, R.; Boskovic, C.; Chaboussant, G.; Güdel, H. U.; Murrie, M.; Ochsenbein, S. T.; Sieber, A. Molecular Spin Clusters: New Synthetic Approaches and Neutron Scattering Studies. *ChemPhysChem* **2003**, *4*, 910−926.

(27) Wang, S. L.; Li, L.; Ouyang, Z. W.; Xia, Z. C.; Xia, N. M.; Peng, T.; Zhang, K. B. Development of high-magnetic-field, high frequency electronic spin resonance system. *Acta Phys. Sin.* **2012**, *61*, 107601.

(28) Nojiri, H.; Ouyang, Z. W. THz Electron Spin Resonance on Nanomagnets. *Terahertz Sci. Technol.* **2012**, *5*, 1−10.

(29) Karlstrom, G.; Lindh, R.; Malmqvist, P. A.; Roos, B. O.; Ryde, U.; Veryazov, V.; Widmark, P. O.; Cossi, M.; Schimmelpfennig, B.; Neogrady, P.; Seijo, L. MOLCAS: a program package for computational chemistry. *Comput. Mater. Sci.* **2003**, *28*, 222−239.

(30) Neese, F. *ORCA-an ab initio, density functional and semiempirical program package, Version 3.03*; Max-Planck institute for bioinorganic chemistry, Mülheim an der Ruhr, Germany, 2016.

(31) Angeli, C.; Bories, B.; Cavallini, A.; Cimiraglia, R. Third-order multireference perturbation theory: The n-electron valence state perturbation-theory approach. *J. Chem. Phys.* **2006**, *124*, 054108.

(32) Hess, B. A.; Marian, C. M.; Wahlgren, U.; Gropen, O. A mean-field spin-orbit method applicable to correlated wavefunctions. *Chem. Phys. Lett.* **1996**, *251*, 365−371.

(33) Weigend, F.; Ahlrichs, R. Balanced basis sets of split valence, triple zeta valence and quadruple zeta valence quality for H to Rn: Design and assessment of accuracy. *Phys. Chem. Chem. Phys.* **2005**, *7*, 3297−3305.

(34) Addison, C. C.; Logan, N.; Wallwork, S. C. Structural Aspects of Co-ordinated Nitrate Groups. *Q. Rev., Chem. Soc.* **1971**, *25*, 289−322.

(35) (a) Casanova, D.; Alemany, P.; Bofill, J. M.; Alvarez, S. Shape and Symmetry of Heptacoordinate Transition-Metal Complexes: Structural Trends. *Chem. - Eur. J.* **2003**, *9*, 1281−1295. (b) Casanova, D.; Llunell, M.; Alemany, P.; Alvarez, S. The Rich Stereochemistry of Eight-Vertex Polyhedra: A Continuous Shape Measures Study. *Chem. - Eur. J.* **2005**, *11*, 1479−1494.

(36) Chilton, N. F.; Anderson, R. P.; Turner, L. D.; Soncini, A.; Murray, K. S. PHI: A Powerful New Program for the Analysis of Anisotropic Monomeric and Exchange-Coupled Polynuclear d- and f-Block Complexes. *J. Comput. Chem.* **2013**, *34*, 1164−1175.

(37) Reviews: (a) Amoretti, G.; Caciuffo, R.; Carretta, S.; Guidi, T.; Magnani, N.; Santini, P. Inelastic neutron scattering investigations of molecular nanomagnets. *Inorg. Chim. Acta* **2008**, *361*, 3771−3776. (b) Baker, M. L.; Mutka, H. Neutron spectroscopy of molecular nanomagnets. *Eur. Phys. J.: Spec. Top.* **2012**, *213*, 53−68. (c) Furrer, A. Magnetic Cluster Excitations. *Int. J. Mod. Phys. B* **2010**, *24*, 3653−3691. (d) Furrer, A.; Waldmann, O. Magnetic cluster excitations. *Rev. Mod. Phys.* **2013**, *85*, 367−420. (e) Bircher, R.; Chaboussant, G.; Dobe, C.; Güdel, H. U.; Ochsenbein, S. T.; Sieber, A.; Waldmann, O. Single-Molecule Magnets Under Pressure. *Adv. Funct. Mater.* **2006**, *16*, 209−220.

(38) (a) Andres, H.; Basler, R.; Güdel, H.-U.; Aromi, G.; Christou, G.; Büttner, H.; Ruffle, B. Inelastic Neutron Scattering and Magnetic Susceptibilities of the Single-Molecule Magnets $[Mn_4O_3X(OAc)_3(dbm)_3]$(X = Br, Cl, OAc, and F): Variation of the Anisotropy along the Series. *J. Am. Chem. Soc.* **2000**, *122*, 12469−12477. (b) Basler, R.; Sieber, A.; Chaboussant, G.; Güdel, H. U.; Chakov, N. E.; Soler, M.; Christou, G.; Desmedt, A.; Lechner, R. Inelastic Neutron Scattering Study of Electron Reduction in Mn_{12} Derivatives. *Inorg. Chem.* **2005**, *44*, 649−653. (c) Piligkos, S.; Rajaraman, G.; Soler, M.; Kirchner, N.; van Slageren, J.; Bircher, R.; Parsons, S.; Güdel, H.-U.; Kortus, J.; Wernsdorfer, W.; Christou, G.; Brechin, E. K. Studies of an Enneanuclear Manganese Single-Molecule Magnet. *J. Am. Chem. Soc.* **2005**, *127*, 5572−5580. (d) Clemente-Juan, J. M.; Coronado, E.

DOI: 10.1021/acs.inorgchem.6b01544
Inorg. Chem. 2016, 55, 12603−12617

Magnetic clusters from polyoxometalate complexes. *Coord. Chem. Rev.* **1999**, *193*−*195*, 361−394. (e) Blake, A. B.; Anson, C. E.; arapKoske, S. K.; Cannon, R. D.; Jayasooriya, U. A.; Saad, A. K.; White, R. P.; Summerfield, D. Inelastic neutron scattering measurements on $[Cu_4OCl_6L_4]$ (L = pyridine or dimethyl sulfoxide). Observation of zero-field splitting of the cluster ground state. *J. Chem. Soc., Dalton Trans.* **1997**, 2039−2043. (g) Clemente-Juan, J. M.; Andres, H.; Borrás-Almenar, J. J.; Coronado, E.; Güdel, H. U.; Aebersold, M.; Kearly, G.; Büttner, H.; Zolliker, M. Magnetic Excitations in Polyoxometalate Clusters Observed by Inelastic Neutron Scattering: Evidence for Ferromagnetic Exchange Interactions and Spin Anisotropy in the Tetrameric Nickel(II) Cluster $[Ni_4(H_2O)_2(PW_9O_{34})_2]^{10-}$ and Comparison with the Magnetic Properties. *J. Am. Chem. Soc.* **1999**, *121*, 10021−10027.

(39) Selected examples of INS applications in mononuclear metal complexes: (a) Kittilstved, K. R.; Sorgho, L. A.; Amstutz, N.; Tregenna-Piggott, P. L.W.; Hauser, A. Ground-State Electronic Structure of Vanadium(III) Trisoxalate in Hydrated Compounds. *Inorg. Chem.* **2009**, *48*, 7750−7764. (b) Dobe, C.; Noble, C.; Carver, G.; Tregenna-Piggott, P. L. W.; McIntyre, G. J.; Barra, A.-L.; Neels, A.; Janssen, S.; Juranyi, F. Electronic and Molecular Structure of High-Spin d^4 Complexes: Experimental and Theoretical Study of the $[Cr(D_2O)_6]^{2+}$ Cation in Tutton's Salts. *J. Am. Chem. Soc.* **2004**, *126*, 16639−16652. (c) Basler, R.; Tregenna-Piggott, P. L. W.; Andres, H.; Dobe, C.; Güdel, H.-U.; Janssen, S.; McIntyre, G. J. Magnetic Excitations of $CsMn(SO_4)_2{\cdot}2D_2O$, Measured by Inelastic Neutron Scattering. *J. Am. Chem. Soc.* **2001**, *123*, 3377−3378. (d) Carver, G.; Tregenna-Piggott, P. L. W.; Barra, A.-L.; Neels, A.; Stride, J. A. Spectroscopic and Structural Characterization of the $[Fe(imidazole)^6]^{2+}$ Cation. *Inorg. Chem.* **2003**, *42*, 5771−5777. (e) Hunter, S. C.; Podlesnyak, A. A.; Xue, Z.-L. Magnetic Excitations in Metalloporphyrins by Inelastic Neutron Scattering: Determination of Zero-Field Splittings in Iron, Manganese, and Chromium Complexes. *Inorg. Chem.* **2014**, *53*, 1955−1961. (f) Stavretis, S. E.; Atanasov, M.; Podlesnyak, A. A.; Hunter, S. C.; Neese, F.; Xue, Z. L. Magnetic Transitions in Iron Porphyrin Halides by Inelastic Neutron Scattering and Ab Initio Studies of Zero-Field Splittings. *Inorg. Chem.* **2015**, *54*, 9790−9801.

(40) (a) Vaknin, D.; Garlea, V. O.; Demmel, F.; Mamontov, E.; Nojiri, H.; Martin, C.; Chiorescu, I.; Qiu, Y.; Kögerler, P.; Fielden, J.; Engelhardt, L.; Rainey, C.; Luban, M. Level crossings and zero-field splitting in the $\{Cr_8\}$-cubane spin cluster studied using inelastic neutron scattering and magnetization. *J. Phys.: Condens. Matter* **2010**, *22*, 466001. (b) Vaknin, D.; Demmel, F. Magnetic spectra in the tridiminished-icosahedron by inelastic neutron scattering. *Phys. Rev. B: Condens. Matter Mater. Phys.* **2014**, *89*, 180411. (c) Garlea, V. O.; Nagler, S. E.; Zarestky, J. L.; Stassis, C.; Vaknin, D.; Kögerler, P.; McMorrow, D. F.; Niedermayer, C.; Tennant, D. A.; Lake, B.; Qiu, Y.; Exler, M.; Schnack, J.; Luban, M. Probing spin frustration in high-symmetry magnetic nanomolecules by inelastic neutron scattering. *Phys. Rev. B: Condens. Matter Mater. Phys.* **2006**, *73*, 024414. (d) Carretta, S.; Santini, P.; Amoretti, G.; Guidi, T.; Copley, J. R. D.; Qiu, Y.; Caciuffo, R.; Timco, G.; Winpenny, R. E. P. Quantum Oscillations of the Total Spin in a Heterometallic Antiferromagnetic Ring: Evidence from Neutron Spectroscopy. *Phys. Rev. Lett.* **2007**, *98*, 167401.

(41) (a) Hagiwara, M.; Regnault, L. P.; Zheludev, A.; Stunault, A.; Metoki, N.; Suzuki, T.; Suga, S.; Kakurai, K.; Koike, Y.; Vorderwisch, P.; Chung, J.-H. Spin Excitations in an Anisotropic Bond-Alternating Quantum S = 1 Chain in a Magnetic Field: Contrast to Haldane Spin Chains. *Phys. Rev. Lett.* **2005**, *94*, 177202. (b) Kim, J.-H.; Ji, S.; Lee, S.-H.; Lake, B.; Yildirim, T.; Nojiri, H.; Kikuchi, H.; Habicht, K.; Qiu, Y.; Kiefer, K. External Magnetic Field Effects on a Distorted Kagome Antiferromagnet. *Phys. Rev. Lett.* **2008**, *101*, 107201. (c) Tsyrulin, N.; Pardini, T.; Singh, R. R. P.; Xiao, F.; Link, P.; Schneidewind, A.; Hiess, A.; Landee, C. P.; Turnbull, M. M.; Kenzelmann, M. Quantum Effects in a Weakly Frustrated S = 1/2 Two-Dimensional Heisenberg Antiferromagnet in an Applied Magnetic Field. *Phys. Rev. Lett.* **2009**, *102*, 197201.

(42) (a) Krzystek, J.; Ozarowski, O.; Telser, J. Multi-frequency, high-field EPR as a powerful tool to accurately determine zero-field splitting in high-spin transition metal coordination complexes. *Coord. Chem. Rev.* **2006**, *250*, 2308−2324. (b) Krzystek, J.; Zvyagin, S. A.; Ozarowski, O.; Trofimenko, S.; Telser, J. Tunable-frequency high-field electron paramagnetic resonance. *J. Magn. Reson.* **2006**, *178*, 174−183.

(43) Xavier, F. R.; Neves, A.; Casellato, A.; Peralta, R. A.; Bortoluzzi, A. J.; Szpoganicz, B.; Severino, P. C.; Terenzi, H.; Tomkowicz, Z.; Ostrovsky, S.; Haase, W.; Ozarowski, A.; Krzystek, J.; Telser, J.; Schenk, G.; Gahan, L. R. Unsymmetrical $Fe^{III}Co^{II}$ and $Ga^{III}Co_{II}$ Complexes as Chemical Hydrolases: Biomimetic Models for Purple Acid Phosphatases (PAPs). *Inorg. Chem.* **2009**, *48*, 7905−7921.

(44) (a) Ruamps, R.; Batchelor, L. J.; Maurice, R.; Gogoi, N.; Jiménez-Lozano, P.; Guihéry, N.; de Graaf, C.; Barra, A.-L.; Sutter, J.-P.; Mallah, T. Origin of the Magnetic Anisotropy in Heptacoordinate Ni^{II} and Co^{II} Complexes. *Chem. - Eur. J.* **2013**, *19*, 950−956. (b) Platas-Iglesias, C.; Vaiana, L.; Esteban-Gómez, D.; Avecilla, F.; Real, J. A.; de Blas, A.; Rodrígue-Blas, T. Electronic Structure Study of Seven-Coordinate First-Row Transition Metal Complexes Derived from 1,10-Diaza-15-crown-5: A Successful Marriage of Theory with Experiment. *Inorg. Chem.* **2005**, *44*, 9704−9713. (c) Batchelor, L. J.; Sangalli, M.; Guillot, R.; Guihéry, N.; Maurice, R.; Tuna, F.; Mallah, T. Pentanuclear Cyanide-Bridged Complexes Based on Highly Anisotropic Co^{II} Seven-Coordinate Building Blocks: Synthesis,Structure, and Magnetic Behavior. *Inorg. Chem.* **2011**, *50*, 12045−12052. (d) Schleife, F.; Rodenstein, A.; Kirmse, R.; Kersting, B. Seven-coordinate Mn(II) and Co(II) complexes of the pentadentate ligand 2,6-diacetyl-4-carboxymethyl-pyridine bis(benzoylhydrazone): Synthesis,crystal structure and magnetic properties. *Inorg. Chim. Acta* **2011**, *374*, 521−527. (e) Dey, M.; Dutta, S.; Sarma, B.; Deka, R. C.; Gogoi, N. Modulation of the coordination environment: a convenient approach to tailor magnetic anisotropy in seven coordinate Co(II) complexes. *Chem. Commun.* **2016**, *52*, 753−756.

(45) Simulations were performed using SPIN, developed by Andrew Ozarowski of the National High Magnetic Field Laboratory, USA.

(46) Garner, C. D.; Mabbs, F. E. Studies in Eight-co-ordination. Part IV. Single-crystal Electronic Spectrum and Magnetic Anisotropy of Tetraphenylarsonium Tetrakis(trifluroacetato) cobaltate(II). *J. Chem. Soc., Dalton Trans.* **1976**, 525−528.

(47) (a) Cole, K. S.; Cole, R. H. Dispersion and Absorption in Dielectrics I. Alternating Current Characteristics. *J. Chem. Phys.* **1941**, *9*, 341−351. (b) Aubin, S. M. J.; Sun, Z. M.; Pardi, L.; Krzystek, J.; Folting, K.; Brunel, L. C.; Rheingold, A. L.; Christou, G.; Hendrickson, D. N. Reduced Anionic Mn_{12} Molecules with Half-Integer Ground States as Single-Molecule Magnets. *Inorg. Chem.* **1999**, *38*, 5329−5340.

(48) Carlin, R. L.; van Duyneveldt, A. J. *Magnetic Properties of Transition Metal Compounds*; Springer-Verlag: New York, 1976.

(49) Schwoerer, M.; Wolf, H. C. Molecular and Lattice Dynamics in Organic Molecular Crystals. In *Organic Molecular Crystals*; Wiley-VCH: Weinheim, Germany, 2007; Chapter 5, pp 89−124.

(50) Tesi, L.; Lunghi, A.; Atzori, M.; Lucaccini, E.; Sorace, L.; Totti, F.; Sessoli, R. Giant spin-phonon bottleneck effects in evaporable vanadyl-based molecules with long spin coherence. *Dalton Trans.* **2016**, *45*, 16635.

(51) Carretta, S.; Santini, P.; Amoretti, G.; Guidi, T.; Dyson, J.; Caciuffo, R.; Stride, J. A.; Caneschi, A.; Copley, J. R. D. Inelastic-neutron-scattering study of excited spin multiplets and low-energy phonons in the Fe_8 nanomagnet: Implications for relaxation. *Phys. Rev. B: Condens. Matter Mater. Phys.* **2006**, *73*, 144425.

(52) (a) Zadrozny, J. M.; Greer, S. M.; Hill, S.; Freedman, D. E. A flexible iron(II) complex in which zero-field splitting is resistant to structural variation. *Chem. Sci.* **2016**, *7*, 416−423. (b) Fataftah, M. S.; Coste, S. C.; Vlaisavljevich, B.; Zadrozny, J. M.; Freedman, D. E. Transformation of the coordination complex $[Co(C_3S_5)_2]^{2-}$ from a molecular magnet to a potential qubit. *Chem. Sci.* **2016**, *7*, 6160−6166.

(53) (a) Zeng, D.; Ren, M.; Bao, S.-S.; Zheng, L.-M. Tuning the Coordination Geometries and Magnetic Dynamics of $[Ln(hfac)_4]^-$ through Alkali Metal Counterions. *Inorg. Chem.* **2014**, *53*, 795−801.

DOI: 10.1021/acs.inorgchem.6b01544
Inorg. Chem. 2016, 55, 12603−12617

(b) Oyarzabal, I.; Ruiz, J.; Ruiz, E.; Aravena, D.; Seco, J. M.; Colacio, E. Increasing the effective energy barrier promoted by the change of a counteranion in a Zn−Dy−Zn SMM: slow relaxation via the second excited state. *Chem. Commun.* **2015**, *51*, 12353−12356.

DOI: 10.1021/acs.inorgchem.6b01544
Inorg. Chem. 2016, 55, 12603−12617